Supplementary Information

DBU as Base and Ligand in Phosphine-free Ruthenium Complexes for Hydrogenation of CO_2

Andrew Z. Preston,[1] Alexander S. Phearman,[1] Manuel Quiroz,[1] Sarah E. Flowers,[1] Nilakshi Devi,[2] Christopher M. Zall,[2] Eric S. Wiedner,[1,*] Aaron M. Appel,[1] John C. Linehan[1,*]

[1]Catalysis Science Group, Pacific Northwest National Laboratory, P.O. Box 999, Richland, Washington 99352, United States

[2] Department of Chemistry, Sam Houston State University, Huntsville, Texas 77341, United States

* E-mail: eric.wiedner@pnnl.gov; John.Linehan@pnnl.gov

Table of Contents

Experimental Details

General Considerations. Unless stated otherwise, reactions and sample preparation were performed in oven-dried glassware under N_2 in a glovebox. Acetonitrile (MeCN) was purified using an Innovative Technologies PureSolv solvent delivery system using alumina under N_2. CD_3CN was purchased from Cambridge Isotopes, purified by distillation over P_2O_5, and stored over 3 Å molecular sieves. NMR spectra were recorded on a 500 MHz Varian Innova spectrometer with broadband probe, 500 MHz Bruker NEO spectrometer with BBFO broadband probe, or 600 MHz Bruker NEO spectrometer with TCI cryoprobe and were referenced using the residual signal of the solvent or to an internal standard. The temperature of the NMR sample probe was calibrated using the difference in shift of the CH_2 and OH resonances of ethylene glycol in a PEEK NMR tube for catalysis studies and using 4% CH_3OH in CD_3OD for low temperature studies. Unless otherwise specified, NMR spectra were collected at 25 °C.

High-Pressure NMR Scale Catalytic Reactions. Hydrogenation reactions were performed using PEEK high-pressure NMR spectroscopy tubes designed and built at Pacific Northwest National Laboratory[1, 2] and with zirconia cells purchased from Daedalus Innovations. In a typical experiment, 50 µL of a 10 mM catalysis solution was mixed with 50 µL of DBU (670 mM), 25 µL of 1,3,5-trimethylbenzene (used as the internal standard), and 375 µL of CD_3CN, resulting in a final ruthenium concentration of 1 mM. Some of the kinetic runs were performed using a sealed capillary of D_2O with $CoCl_2$ as an integration standard, where $CoCl_2$ serves as a paramagnetic relaxation agent and chemical shift agent to decrease the T1 of residual HDO and shift its resonance to an unobscured region of the spectrum (~11.4 ppm).[3] The sample preparation was performed under inert atmosphere in a glovebox, and then the NMR cell was sealed and removed from the glovebox. The amount of internal standard was determined by integration relative to DBU prior to pressurizing with H_2/CO_2. The cells were then connected to a purged high-pressure line connected to an ISCO syringe pump containing 1:1 H_2/CO_2 at a constant pressure and a vacuum pump. The headspace of the cell was degassed by brief introduction of static vacuum (3 × ~10 s), and the gas mixture was introduced while being mixed using a vortex mixer until the pressure had stabilized. The cell was then inserted into the spectrometer.

^{1}H NMR spectra for high-pressure experiments were acquired on a Varian or Bruker 500 MHz spectrometer, using 8 scans for each spectrum. The acquisition time was set to 5 s, the delay time was 1 s, and the pulse width was 2 µs. For the Bruker experiments, a flip angle of 2° was used to obtain quantitative ^{1}H NMR spectra. Each spectrum required 48 s (Varian) or 60 s (Bruker) total to complete, and array functions to introduce a pre-acquisition delay time were utilized to acquire spectra at regular intervals. To ensure adequate gas-liquid mixing, the NMR cell was removed from the spectrometer between each spectrum and shaken on a vortex mixer. The concentration of formate was determined by integration of the formate resonance compared to the known concentration of the internal standard.

NMR Data for Ru species.

$[CpRu(DBU)(NCCH_3)_2][PF_6]$ (**1b**): **^{1}H NMR** (600 MHz, CD_3CN, 25 °C) δ 4.07 (s, 5H), 3.46 (t, *J* = 5.5 Hz, 2H), 3.37 – 3.30 (m, 2H), 3.27 (t, *J* = 6.4 Hz, 2H), 3.06 – 2.92 (m, 2H), 1.76 (p, *J* = 6.1 Hz, 2H), 1.69 - 1.64 (m, 2H), 1.60 – 1.55 (m, 4H). I**nverse gated, quantitative ^{13}C{^{1}H} NMR** (151 MHz, CD_3CN, 25 °C) δ 168.2 (1C), 68.7 (5C, Cp), 54.2 (1C), 53.7 (1C), 49.1 (1C), 38.6 (1C), 30.0 (1C), 28.3 (1C), 27.2 (1C), 23.6 (1C).

$[CpRu(DBU)_2(NCCH_3)][PF_6]$ (**1c**): **^{1}H NMR** (600 MHz, CD_3CN, 25 °C) δ 3.92 (Cp). **Inverse gated, quantitative ^{13}C{^{1}H} NMR** (151 MHz, CD_3CN, -35 °C, 1.30 M DBU) δ 167.1 (2C), 67.8 (5C, Cp), 53.6 (4C), 48.4 (2C), 36.7 (2C), 29.9 (2C), 27.9 (2C), 26.6 (2C), 23.5 (2C).

$[Cp^*Ru(DBU)(NCCH_3)_2][PF_6]$ (**2b**): **^{1}H NMR** (600 MHz, CD_3CN, 25 °C) δ 3.36 (t, *J* = 5.5 Hz, 2H), 3.33 – 3.28 (m, 2H), 3.25 (t, *J* = 6.3 Hz, 2H), 2.88 (dd, *J* = 8.1, 3.5 Hz, 2H), 1.75 (p, *J* = 6.2 Hz, 2H), 1.68 – 1.63 (m, 2H), 1.59 – 1.54 (m, 4H), 1.51 (s, 15H, Cp*). **Inverse gated, quantitative ^{13}C{^{1}H} NMR** (151 MHz, CD_3CN, 25 °C) δ 167.3 (1C), 78.6 (5C, Cp* arene), 54.2 (1C), 52.2 (1C), 49.0 (1C), 38.1 (1C), 30.2 (1C), 28.5 (1C), 27.8 (1C), 24.2 (1C), 9.8 (5C, Cp* methyl).

$[Cp^*Ru(DBU)_2(NCCH_3)][PF_6]$ (**2c**): **Inverse gated, quantitative ^{13}C{^{1}H} NMR** (151 MHz, CD_3CN, −35 °C) δ 72.7 (5C, Cp* arene), 10.5 (5C, Cp* methyl). Note: Only the Cp* resonances of **2c** were observable due to its low population and rapid exchange of the DBU and CD_3CN ligands. No resonances for **2c** were observed by ^{1}H NMR spectroscopy due to overlap with the DBU co-solvent.

X-ray Crystallography. Single crystals of $[Cp^*Ru(DBU)(NCCH_3)_2][PF_6]$ (**2b**) were obtained by vapor diffusion of diethyl ether into a concentrated MeCN/DBU solution of $[Cp^*Ru(NCCH_3)_3][PF_6]$ **2**. A suitable crystal was selected using a microscope and mounted on a cryoloop using ParatoneN oil. Data was collected at 100 K on a Bruker KAPPA APEX III diffractometer equipped with an APEX III CCD detector using a TRIUMPH monochromator with a Mo Kα X-ray source (α = 0.71073 Å). Preliminary indexing was performed from a series of thirty-six 0.5° rotation frames with exposures of 20 seconds. A total of 2504 frames (11 runs) were collected employing ω and ϕ scans with a crystal to detector distance of 50.0 or 46.0 mm, rotation widths of 0.5° and exposures of 27 seconds. Data collection and cell parameter determination were conducted using the SMART program. Integration of the data frames and final cell parameter refinement were performed using SAINT software and absorption correction of the data was carried out using SADABS. Using Olex2,[4] the structure was solved with the SHELXT[5] structure solution program using Intrinsic Phasing and refined with the SHELXL[6] refinement package using Least Squares minimization. All hydrogen atom positions were idealized and rode on the atom of attachment. The asymmetric unit contains one molecule of $[Cp^*Ru(DBU)(NCCH_3)_2][PF_6]$ and a molecule of Et_2O. Minor disorder of the PF_6^- anion is observed, along with rotational disorder of the Cp* ligand (Table S6). Cp* rotational disorder was modeled as two components with occupancies of 0.655(8) and 0.345(8), isotropic restraints, and bond length restraints applied to equivalent C–C bonds in the two Cp* components. PF_6^- anions sit on 2-fold rotation axes. Two of the PF_6^- anions in the unit cell have a 2-fold rotation axis along a F–P–F bonds. The other two PF_6^- anions in the unit cell are disordered about the 2-fold rotation axes and were modeled as two parts. Constraints of several opposing F's were used to set the thermal parameters as equal.

Kinetic Data

Table S1. Summary of TOFs for **1** and **2**.[a]

Entry	Catalyst	$[Ru]_{tot}$ (mM)	$[DBU]_o$ (M)	$[CD_3CN]$ (M) [b]	$[2b]_o$ (mM) [c]	$[2c]_o$ (mM) [c]	P_{H2} (atm)	P_{CO2} (atm)	TOF (h^{-1})
1	**1** (Cp)	0.5	0.67	17.2	0.14	0.36	17	17	850 (3)
2	**2** (Cp*)	0.45	0.61	17.4	0.44	0.01	17	17	320(110)
3	**2** (Cp*)	1.0	0.67	17.2	0.97	0.03	17	17	320 (140)
4	**2** (Cp*)	1.0	0.34	18.2	0.98	0.02	17	17	170 (80)
5	**2** (Cp*)	1.0	1.00	16.3	0.95	0.05	17	17	480 (130)
6	**2** (Cp*)	1.0	1.34	15.3	0.93	0.07	17	17	710 (70)
7	**2** (Cp*)	1.0	0.67	17.2	0.97	0.03	3.4	3.4	100 (40)
8	**2** (Cp*)	0.9	0.61	17.4	0.89	0.03	8.5	25.5	170 [d]
9	**2** (Cp*)	1.0	0.67	17.4	0.97	0.03	13.6	13.6	340 (30)
10	**2** (Cp*)	1.0	0.67	17.4	0.97	0.03	25.5	8.5	300 (2)

[a] All kinetics experiments were performed at 25 °C. TOF values are averaged over 2-3 experiments unless noted otherwise. [b] The concentration of neat CD_3CN is 19.15 M. [c] Calculated from independently measured values of K_1 and K_2. [d] TOF is based on a single measurement.

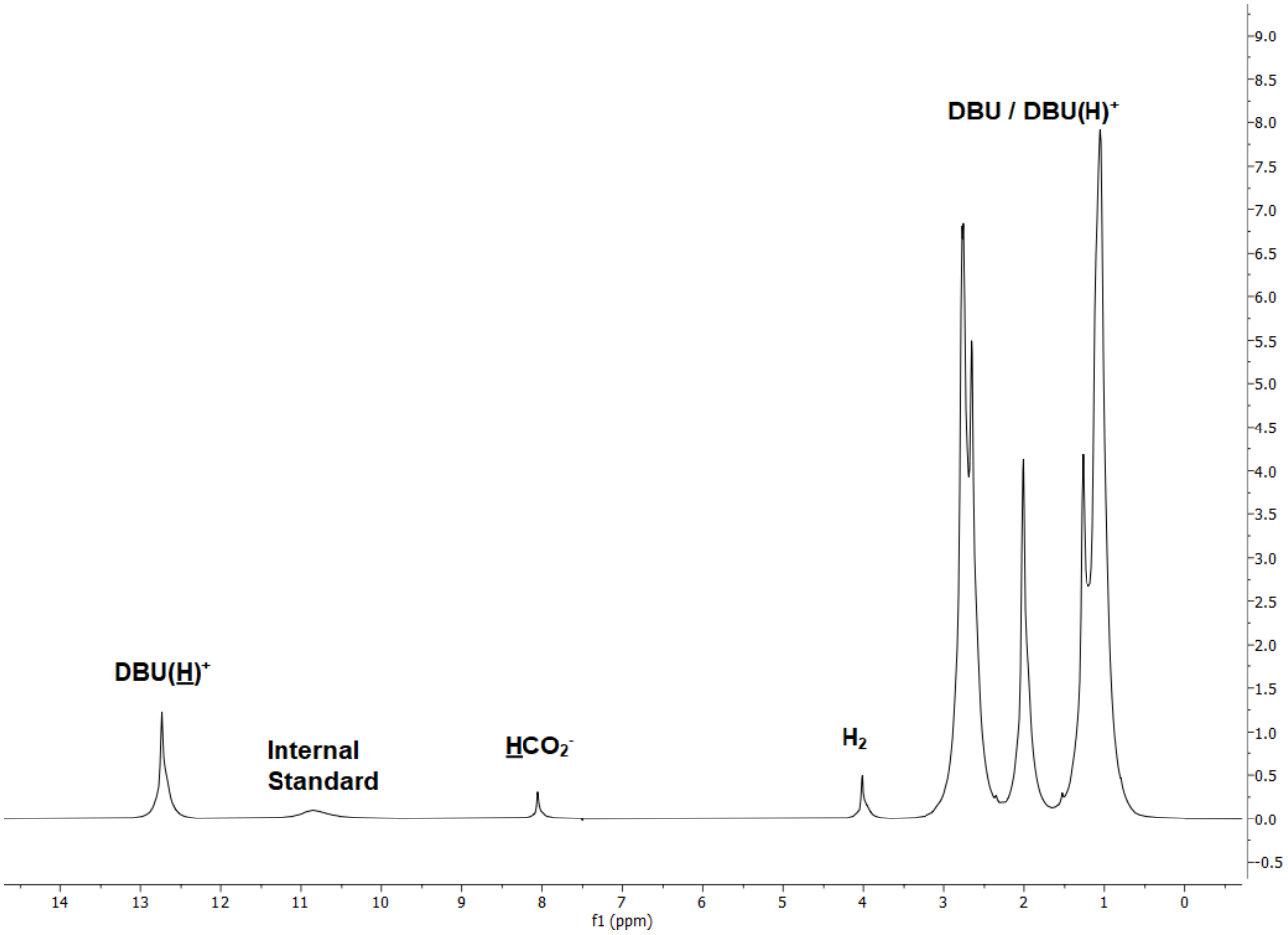

Figure S1. Representative *operando* ^{1}H NMR spectrum (500 MHz, 25 °C) during catalysis using a PEEK NMR cell. Conditions: [**2**] = 0.45 mM, $[DBU]_o$ = 0.61 M, P_{H2} = 17 atm, P_{CO2} = 17 atm, internal standard = $CoCl_2/D_2O$ capillary, timepoint = 1.25 h. In some cases, the apparent amount of $DBU(H)^+$, determined from integration of the "N-H" resonance at ~12.6 ppm, exceeds the amount of formate generated during a catalytic run; this is attributed to adventitious water that leads to the formation of $[DBU(H)^+][HCO_3^-]$ in the presence of CO_2.[7] Similar rates were obtained in the presence and absence of trace water, indicating that the presence of $[DBU(H)^+][HCO_3^-]$ does not impact the rate of catalysis. No resonances for the catalyst were observed due to its low concentration relative to DBU.

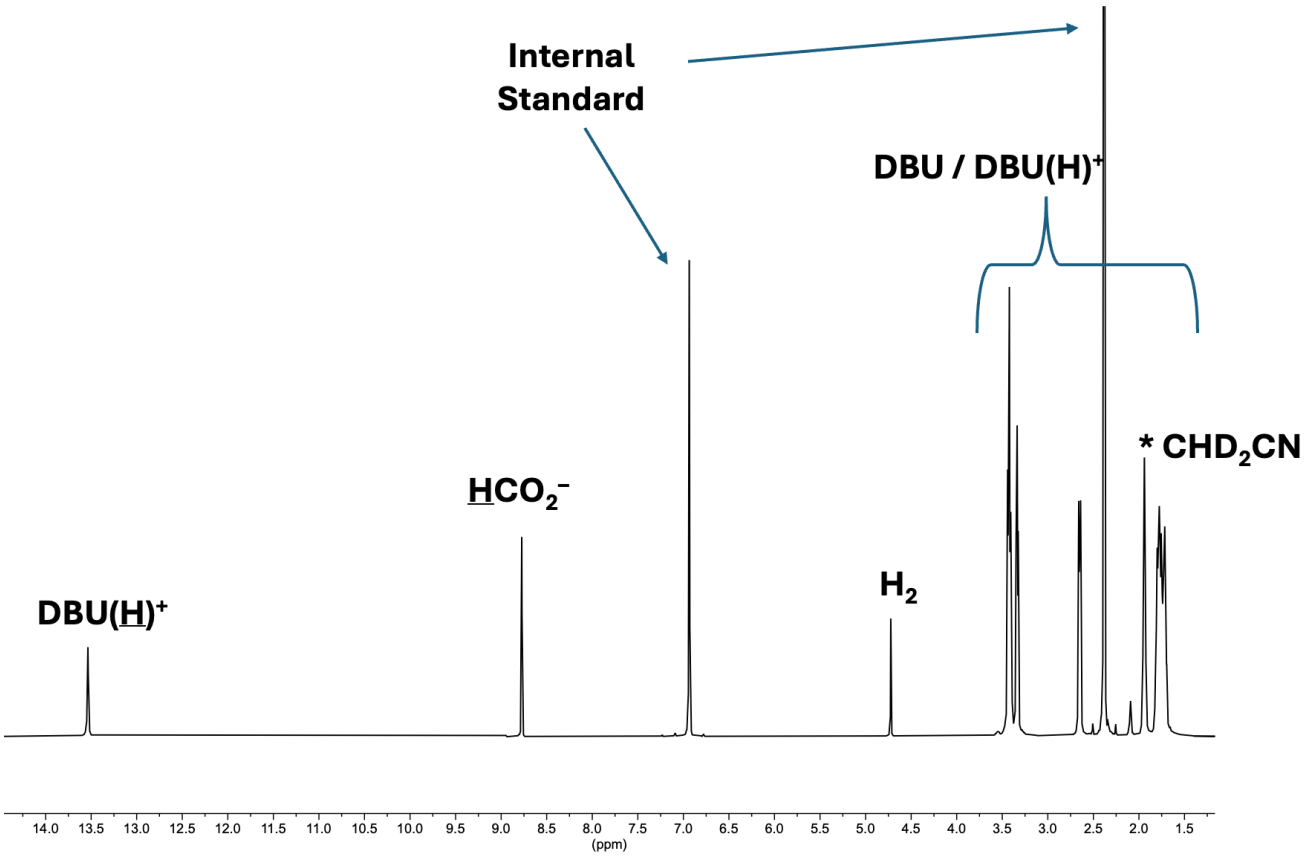

Figure *S*2. Representative operando ^{1}H NMR spectrum (Bruker 500 MHz, 25 °C) during catalysis using a zirconia NMR cell. Conditions: [**1**] = 1 mM, $[DBU]_o$ = 0.67 M, P_{H2} = 17 atm, P_{CO2} = 17 atm, internal standard = 1,3,5-trimethy*l*benzene, timepoint = 1 h. In most cases, the apparent amount of $DBU(H)^+$, as determined by integration of the 'N-H' resonance at ~13.5 ppm, is about the same as the amount of formate produced during a catalytic run with this set up. No resonances for the catalyst were observed due to its low concentration relative to DBU. The resonance for CHD_2CN does not change during the course of the catalytic reaction, indicating that it arises solely from the residual CHD_2CN present in the CD_3CN solvent.

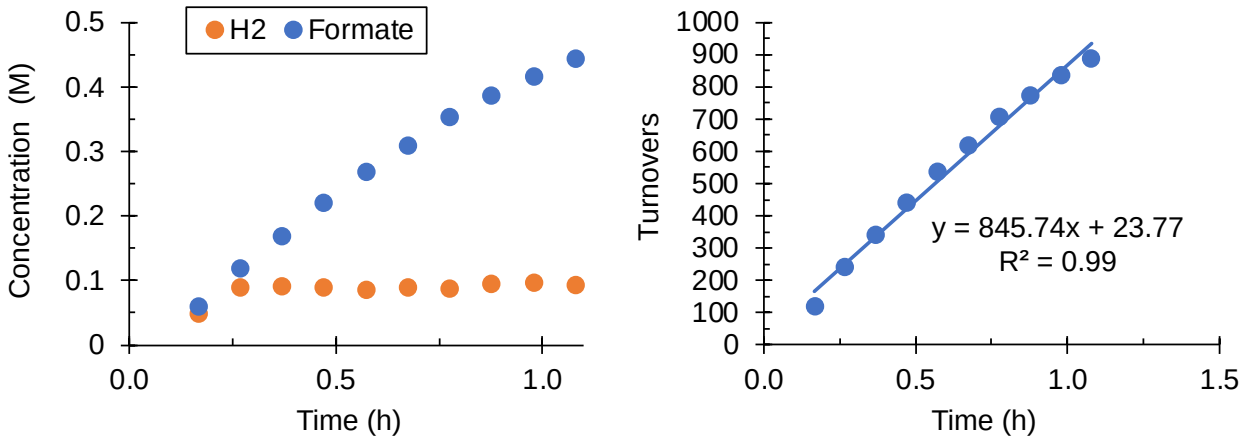

Figure S3. Plots of concentration vs time (left) and turnovers vs time (right) for entry 1 of **Table S1**. Conditions: [**1**] = 0.5 mM, $[DBU]_o$ = 0.67 M, P_{H2} = 17 atm, P_{CO2} = 17 atm, 25 °C.

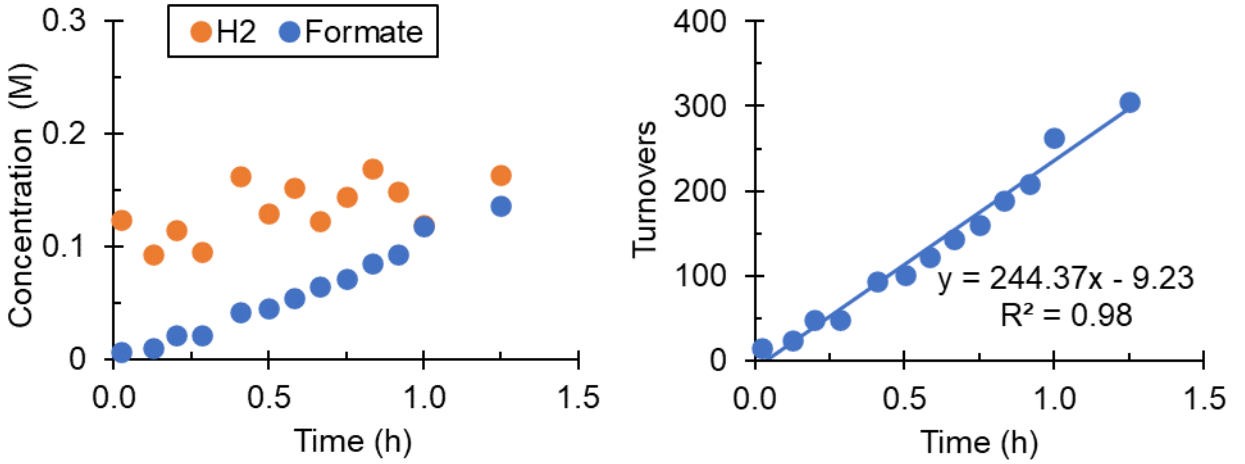

Figure S4. Plots of concentration vs time (left) and turnovers vs time (right) for entry 2 of **Table S1**. Conditions: [**2**] = 0.45 mM, $[DBU]_o$ = 0.61 M, P_{H2} = 17 atm, P_{CO2} = 17 atm, 25 °C.

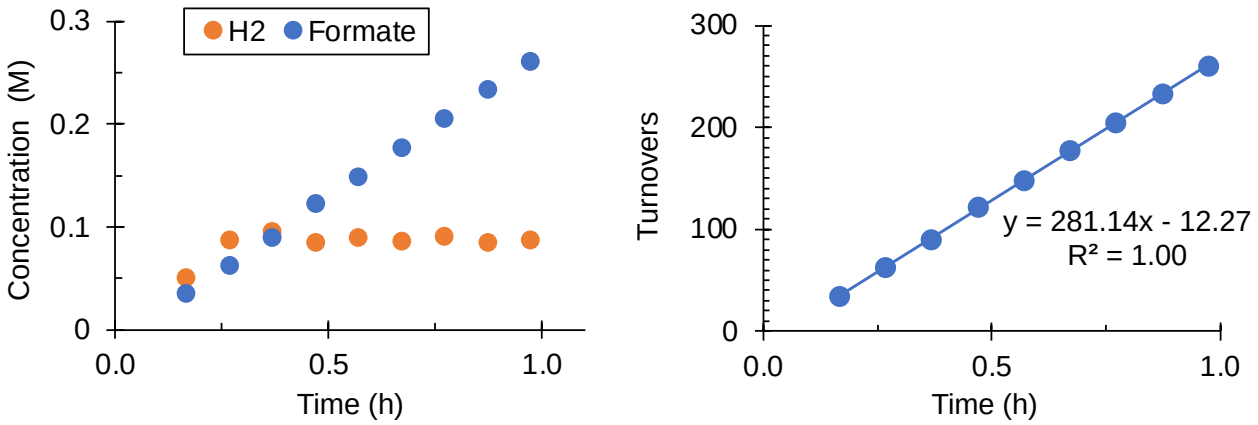

Figure S5. Plots of concentration vs time (left) and turnovers vs time (right) for entry 3 of **Table S1**. Conditions: [**2**] = 1.0 mM, $[DBU]_o$ = 0.67 M, P_{H2} = 17 atm, P_{CO2} = 17 atm, 25 °C.

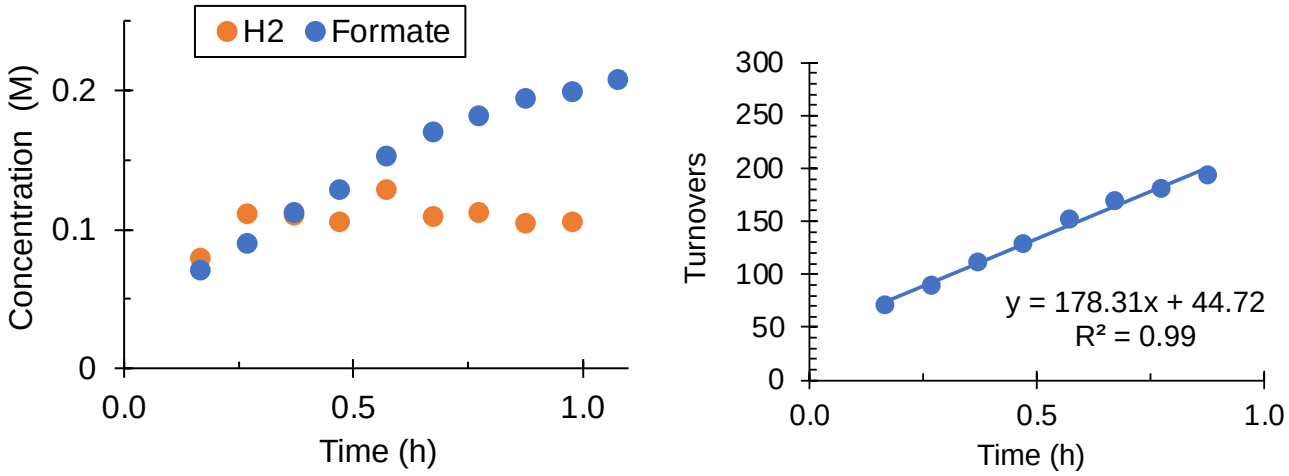

Figure S6. Plots of concentration vs time (left) and turnovers vs time (right) for entry 4 of **Table S1**. Conditions: [**2**] = 1.0 mM, $[DBU]_o$ = 0.34 M, P_{H2} = 17 atm, P_{CO2} = 17 atm, 25 °C.

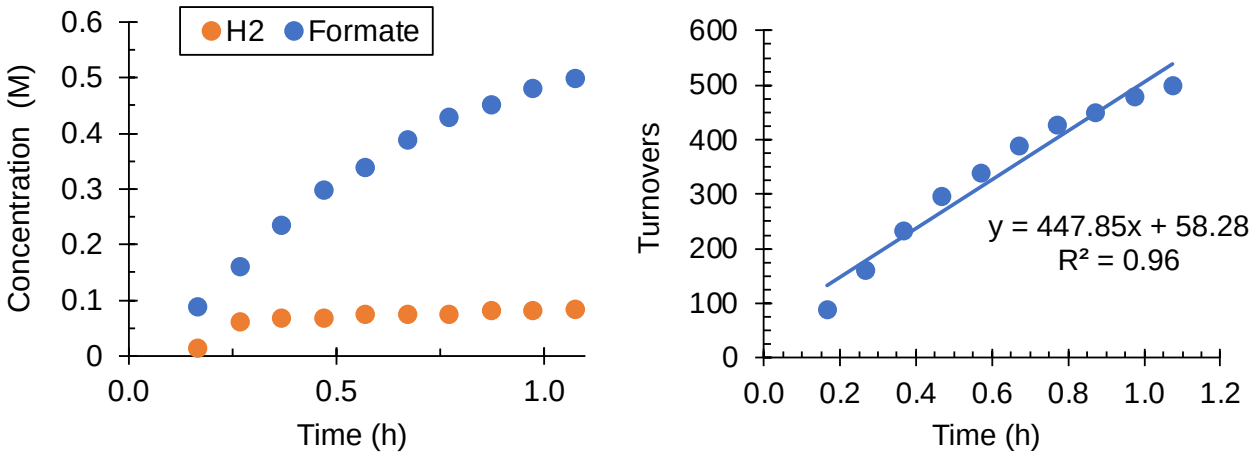

Figure S7. Plots of concentration vs time (left) and turnovers vs time (right) for entry 5 of **Table S1**. Conditions: [**2**] = 1.0 mM, $[DBU]_o$ = 1.00 M, P_{H2} = 17 atm, P_{CO2} = 17 atm, 25 °C.

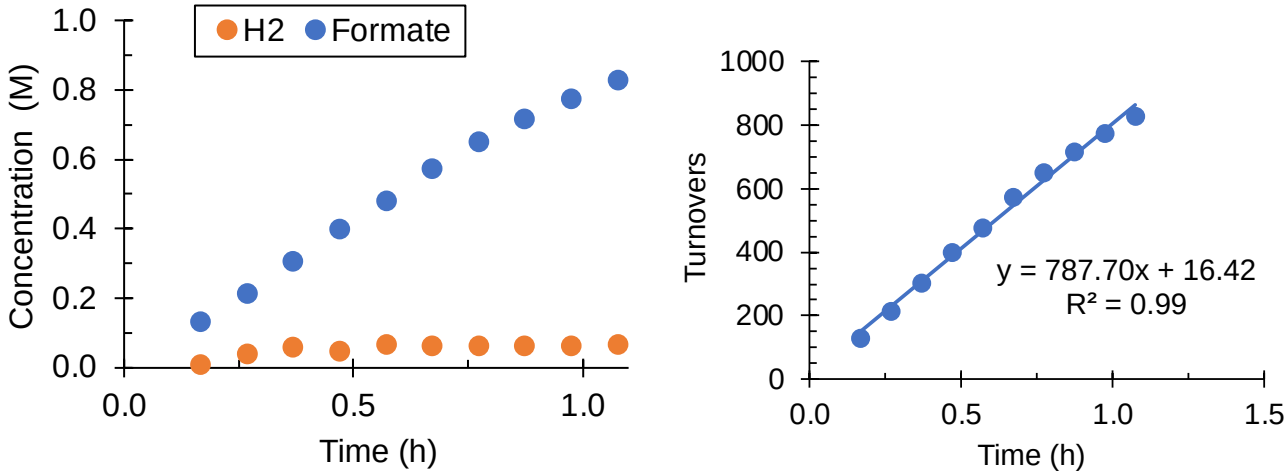

Figure S8. Plots of concentration vs time (left) and turnovers vs time (right) for entry 6 of **Table S1**. Conditions: [**2**] = 1.0 mM, $[DBU]_o$ = 1.34 M, P_{H2} = 17 atm, P_{CO2} = 17 atm, 25 °C.

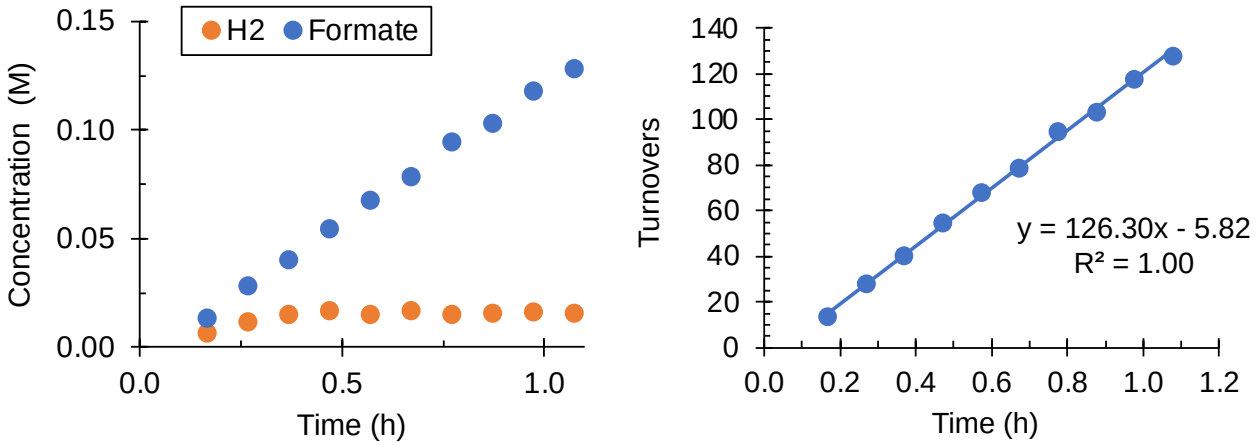

Figure S9. Plots of concentration vs time (left) and turnovers vs time (right) for entry 7 of **Table S1**. Conditions: [**2**] = 1.0 mM, $[DBU]_o$ = 0.67 M, P_{H2} = 3.4 atm, P_{CO2} = 3.4 atm, 25 °C.

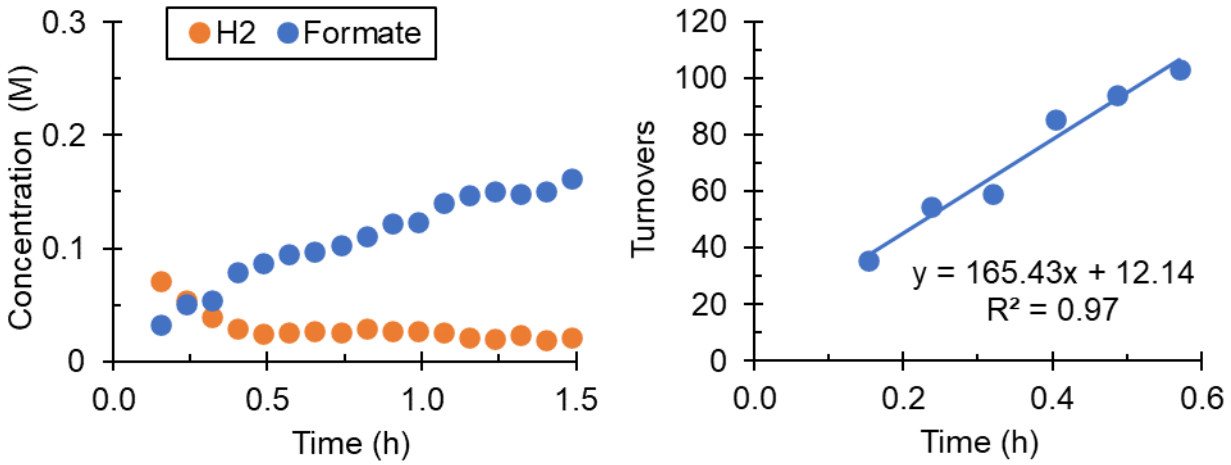

Figure S10. Plots of concentration vs time (left) and turnovers vs time (right) for entry 8 of **Table S1**. Conditions: [**2**] = 0.92 mM, $[DBU]_o$ = 0.61 M, P_{H2} = 8.5 atm, P_{CO2} = 25.5 atm, 25 °C.

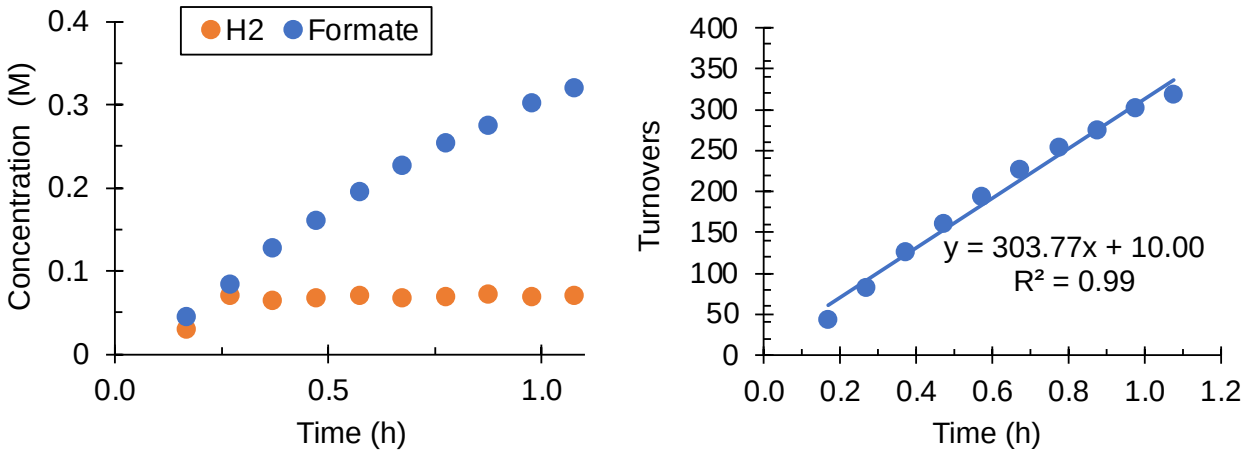

Figure S11. Plots of concentration vs time (left) and turnovers vs time (right) for entry 9 of **Table S1**. Conditions: [**2**] = 1.0 mM, $[DBU]_o$ = 0.67 M, P_{H2} = 13.6 atm, P_{CO2} = 13.6 atm, 25 °C.

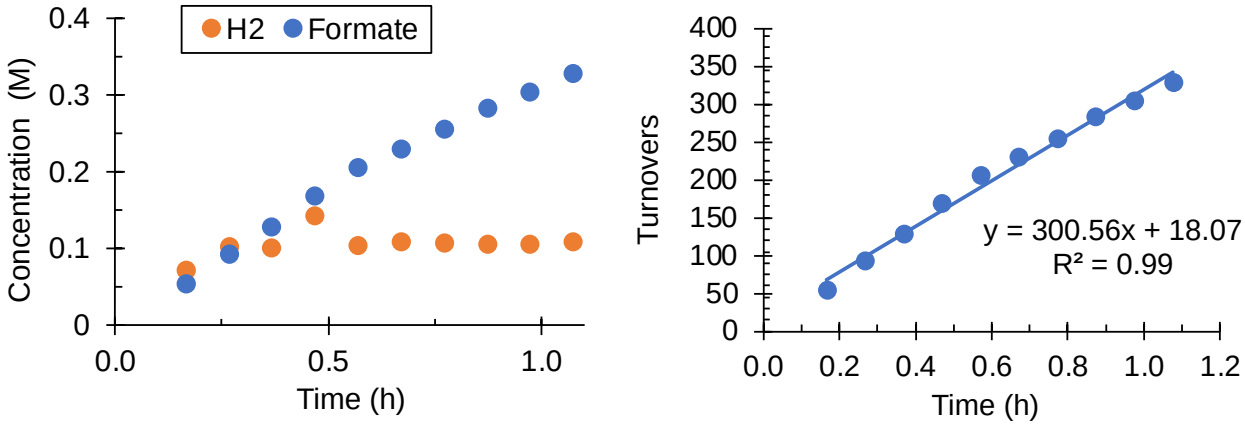

Figure S12. Plots of concentration vs time (left) and turnovers vs time (right) for entry 10 of **Table S1**. Conditions: [**2**] = 1.0 mM, $[DBU]_o$ = 0.67 M, P_{H2} = 25.5 atm, P_{CO2} = 8.5 atm, 25 °C.

*Spectroscopic Characterization of **1b***

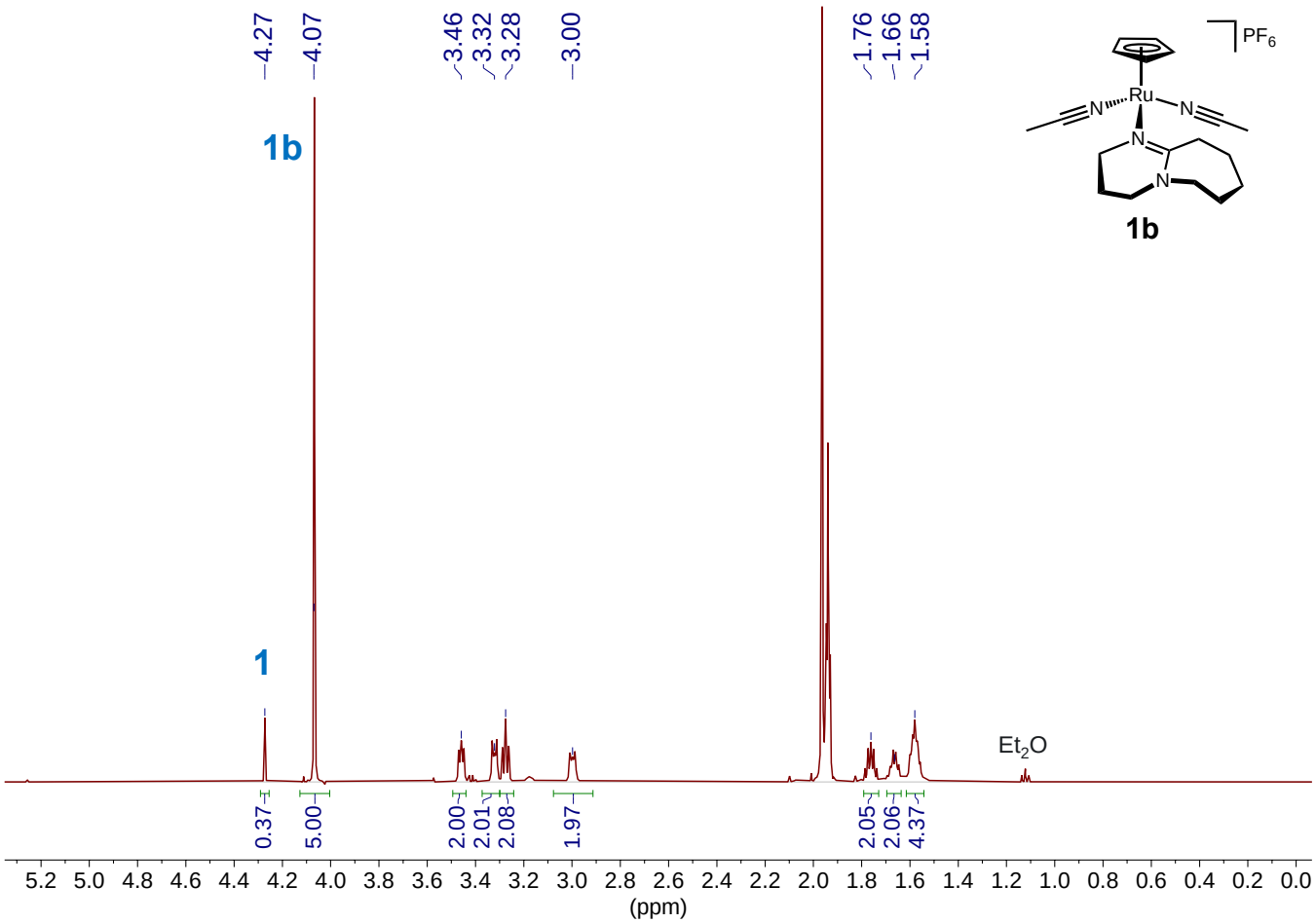

Figure S13. ^{1}H NMR spectrum (500 MHz, CD_3CN, 25 °C) of $[CpRu(NCCH_3)_3]^+$ (**1**, 37.2 mM) with DBU (37.4 mM) showing 93% conversion to **1b** under these conditions.

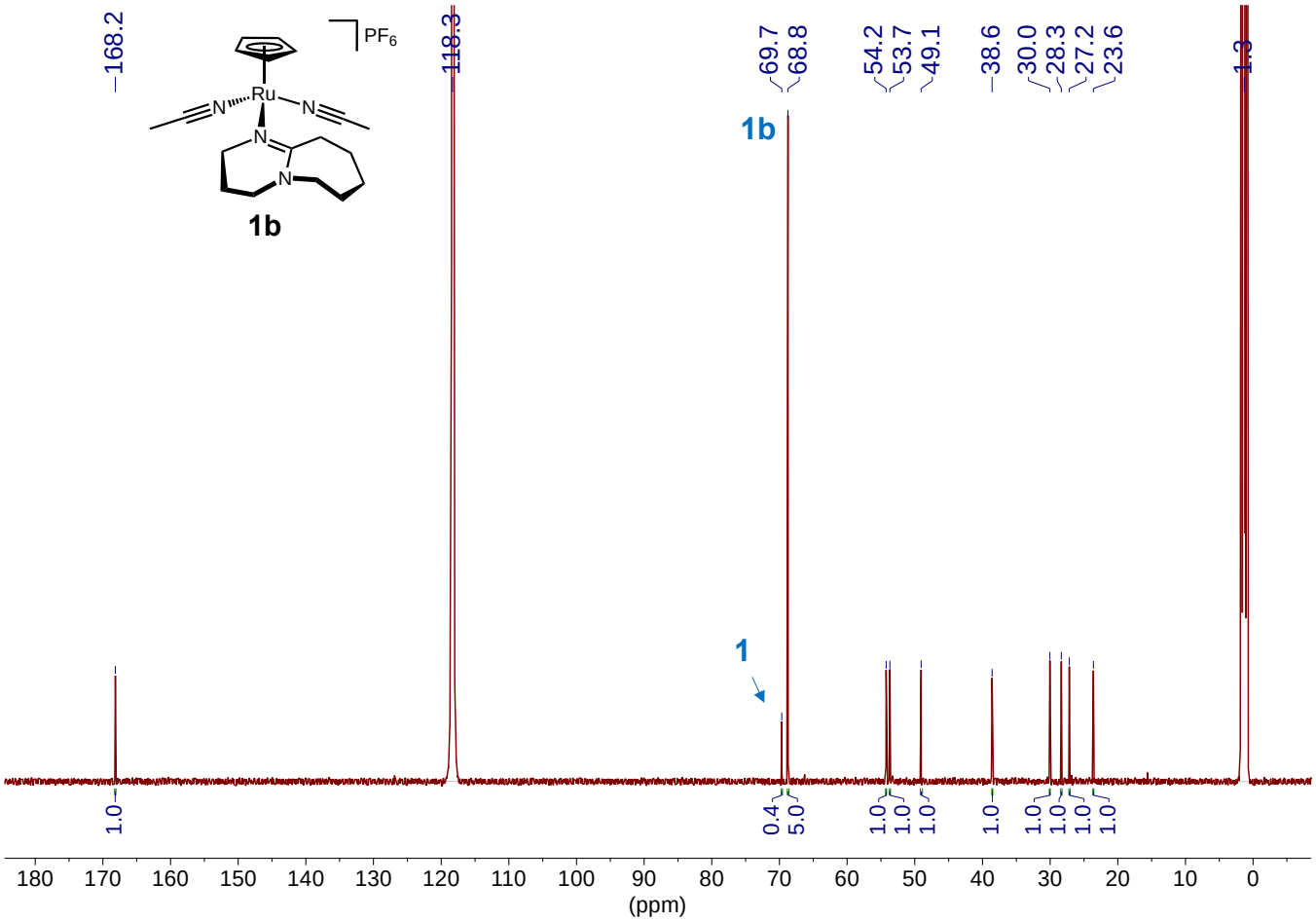

Figure S14. Quantitative $^{13}C\{^{1}H\}$ NMR spectrum (126 MHz, CD_3CN, 25 °C) of $[CpRu(NCCH_3)_3]^+$ (**1**, 37.2 mM)) with DBU (37.4 mM) showing conversion to **1b** under these conditions.

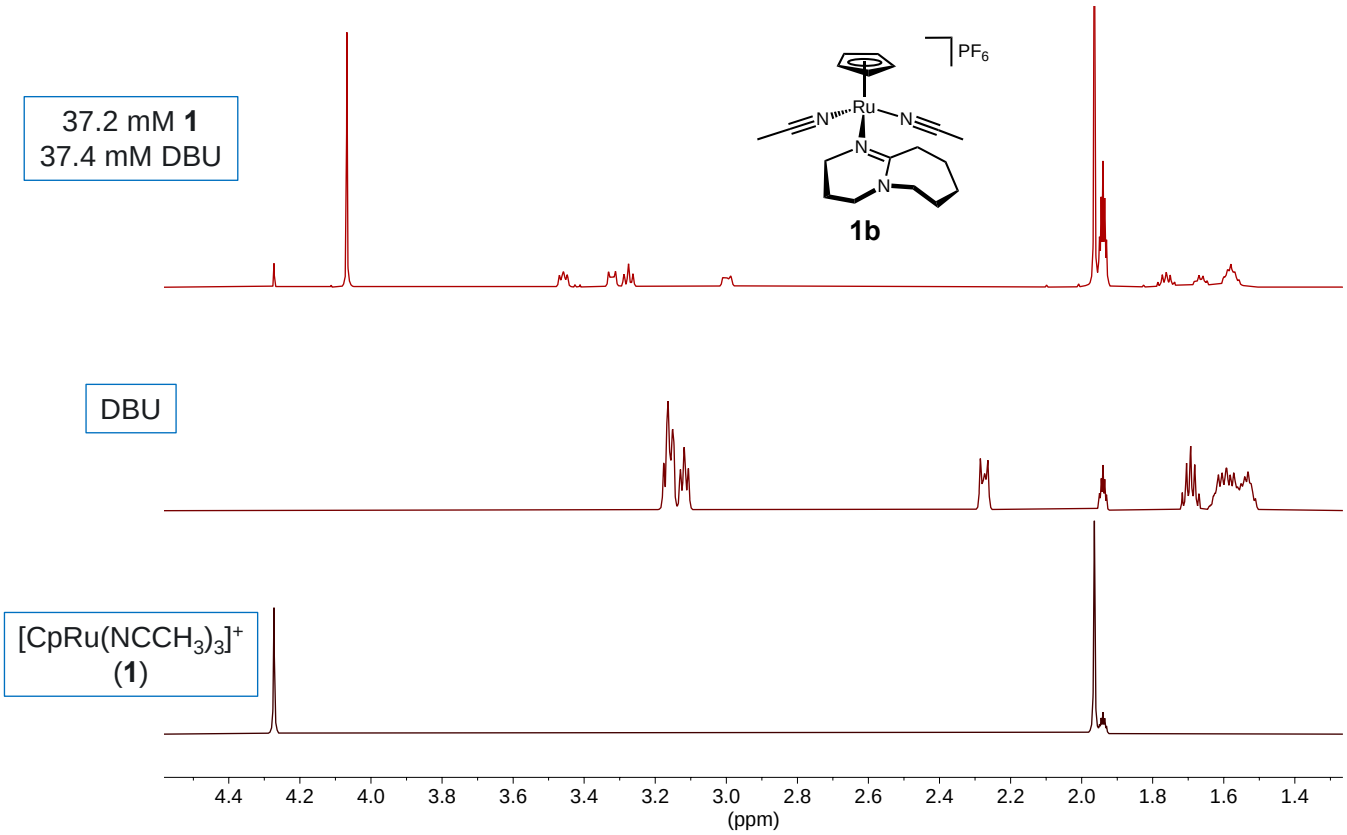

Figure S15. Comparison of partial ^{1}H NMR spectrum (500 MHz, CD_3CN, 25 °C) of $[CpRu(NCCH_3)_3]^+$ (**1**, 37.2 mM)) with DBU (37.4 mM), just DBU, and just **1**, showing shift of DBU and Cp peaks upon formation of **1b**.

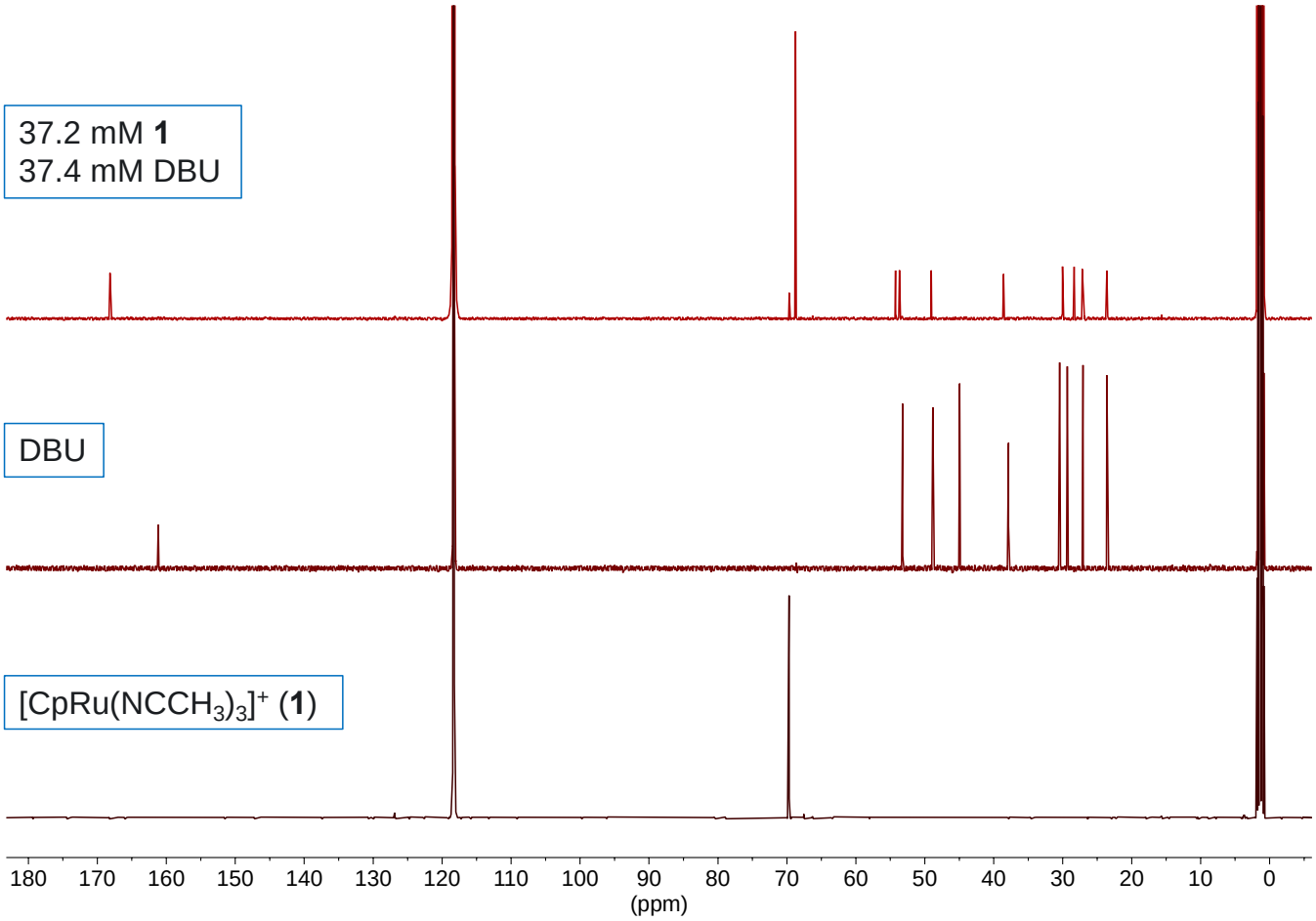

Figure S16. Comparison of $^{13}C\{^{1}H\}$ NMR spectrum (126 MHz, CD_3CN, 25 °C) of $[CpRu(NCCH_3)_3]^+$ (**1**, 37.2 mM)) with DBU (37.4 mM), just DBU, and just **1**, showing shift of DBU and Cp peaks upon formation of **1b**.

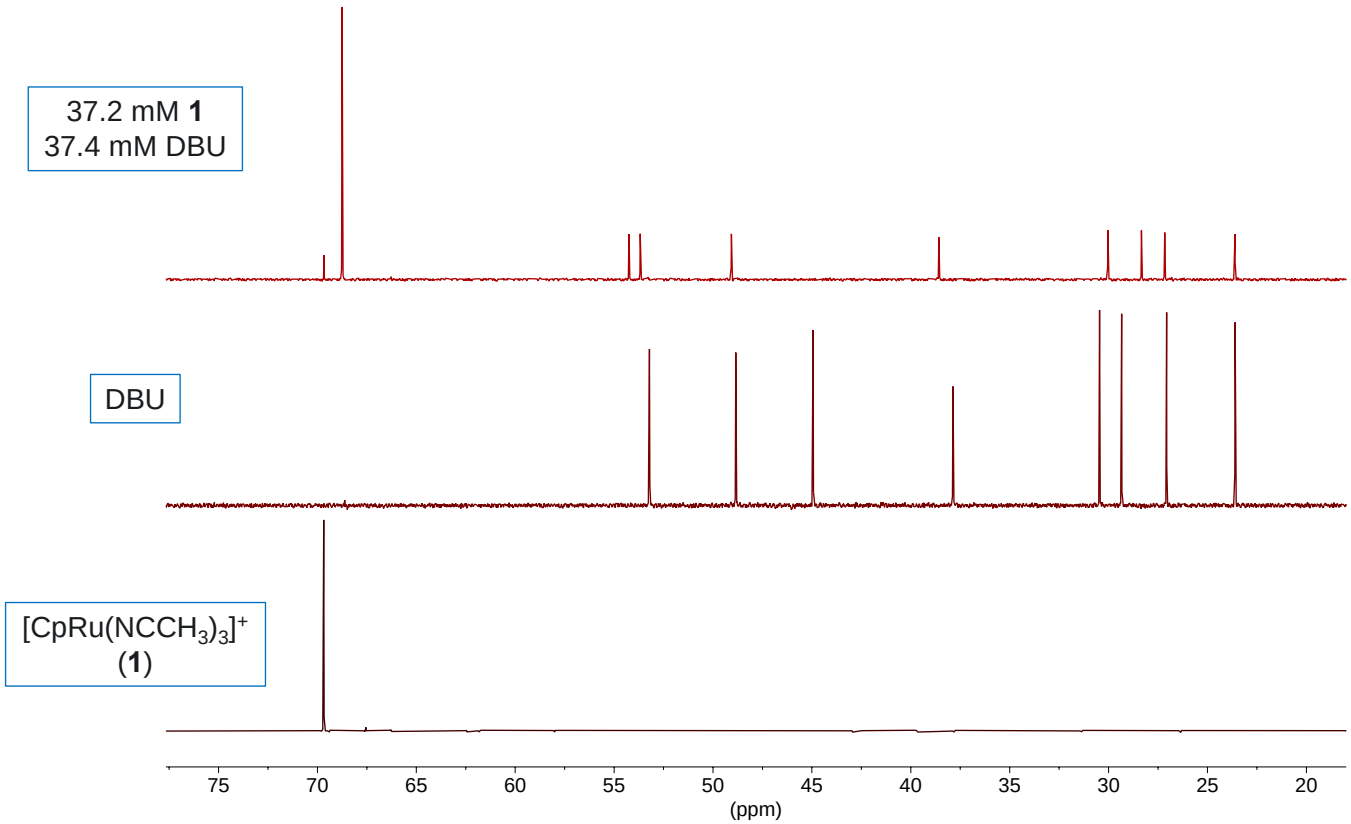

Figure S17. Comparison of partial $^{13}C\{^{1}H\}$ NMR spectrum (126 MHz, CD_3CN, 25 °C) of $[CpRu(NCCH_3)_3]^+$ (**1**, 37.2 mM) with DBU (37.4 mM), just DBU, and just **1**, showing shift of DBU and Cp peaks upon formation of **1b**. Note: these are the same spectra as the previous figure, focusing on the region of 20 – 75 ppm.

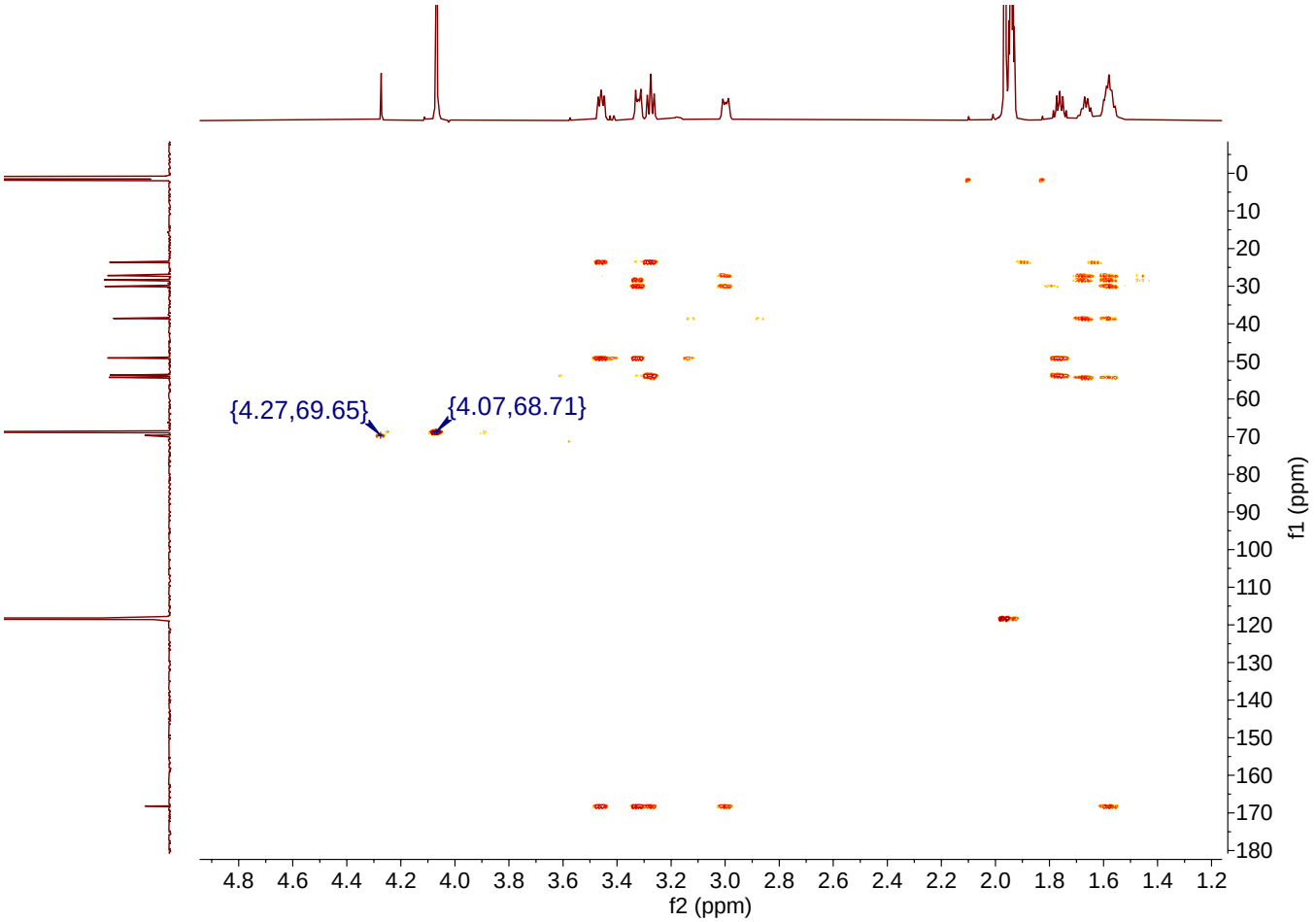

Figure S18. HMBCGP (126/500 MHz, CD_3CN, 25 °C) of $[CpRu(NCCH_3)_3]^+$ (**1**, 37.2 mM) with DBU (37.4 mM). Cross peaks for **1b** (4.07, 68.71 ppm) and **1** (4.27, 69.65 ppm) are emphasized.

*Spectroscopic Characterization of **1c***

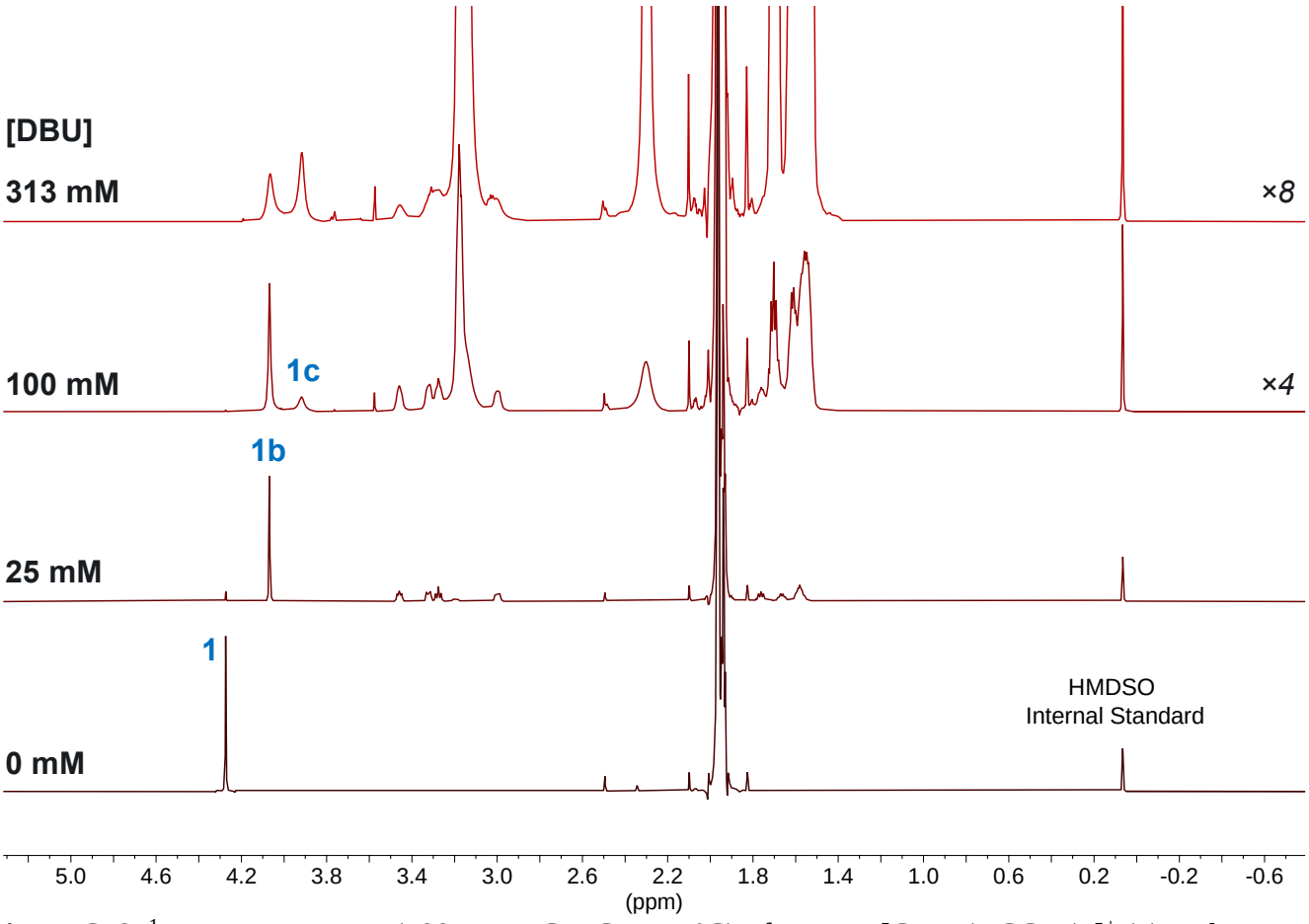

Figure S19. ^{1}H NMR spectrum (500 MHz, CD_3CN, 25 °C) of 25 mM $[CpRu(NCCH_3)_3]^+$ (**1**) with DBU (0-313 mM). **Figure 3** in the main text focuses on the region between 3.80 and 4.40 ppm. In this series of experiments, the CD_3CN concentration sequentially decreases from 19.15 M with no DBU (bottom spectrum) to 19.08 M, 18.86 M, and 18.25 M, respectively, as the DBU concentration increases from 25 mM to 313 mM.

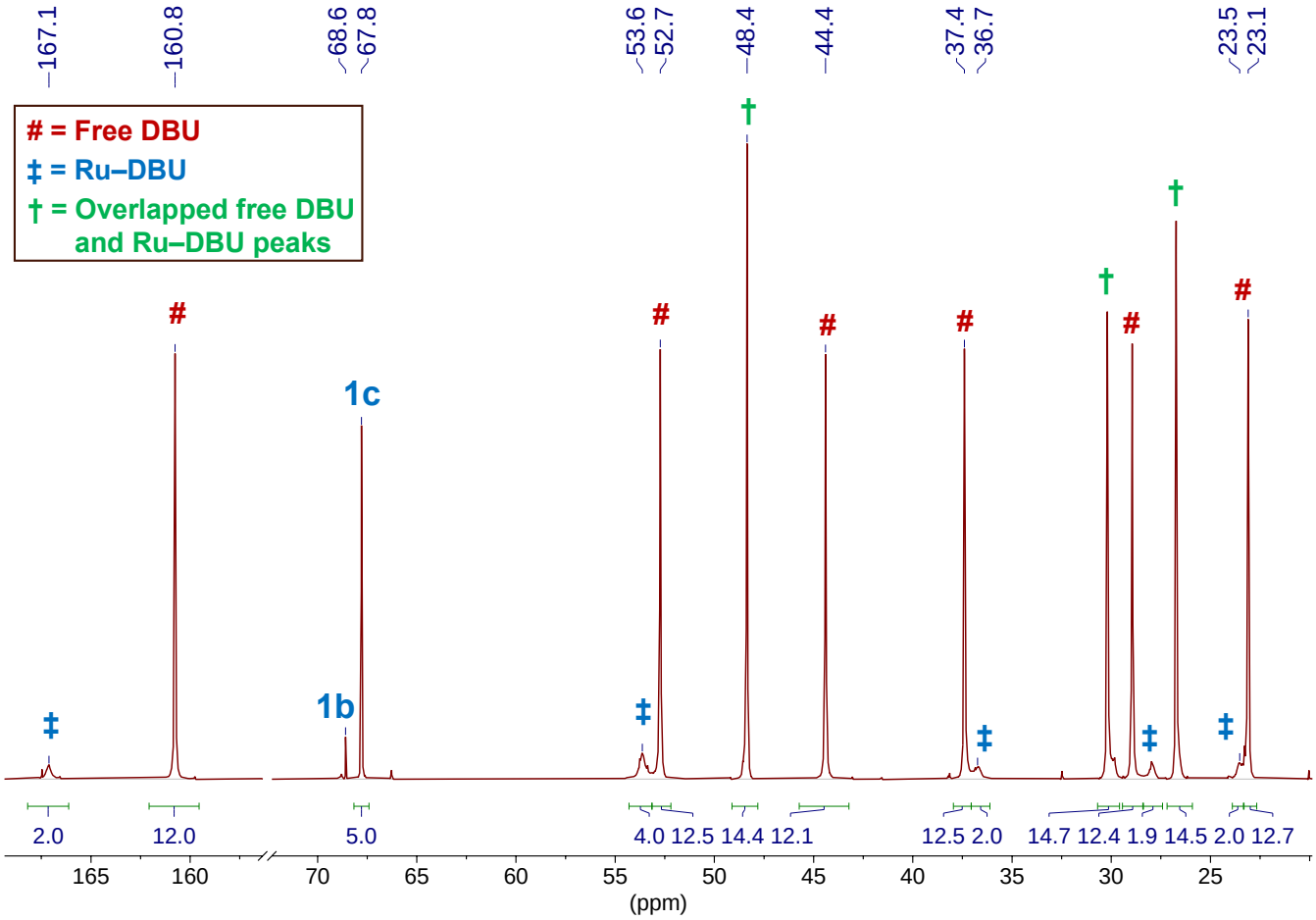

Figure S20. Low temperature inverse gated $^{13}C\{^{1}H\}$ NMR spectrum (151 MHz, CD_3CN, -35 °C) of $[CpRu(NCCH_3)_3]^+$ (**1**) with [DBU] = 1.3 M and $[CD_3CN]$ = 15.4 M showing integration of Ru–DBU signals integrating as 2 DBU per Ru, consistent with the formation of $[CpRu(DBU)_2(NCCH_3)]^+$ under these conditions.

*Exchange Rate for Interconversion of **1b / 1c***

The absolute rate of exchange between **1b** and **1c** with 1.3 M DBU was determined using lineshape analysis, specifically analysis of peak linewidth at half height. For this, the linewidth at 238K was used as a baseline, and the rate of exchange was approximated as too slow to induce measurable line broadening. Thus the linewidth at these temperatures was assumed to be due to field inhomogeneity and inherent relaxation times only, and any additional line broadening at higher temperatures was attributed to the exchange. The initial approximation was done by established methods[8, 9] and refined further using the software gNMR.[10] The resulting fits compared to the collected spectra are shown in Figure S21–Figure S30, and a summary of the absolute rates can be seen in Table S2.

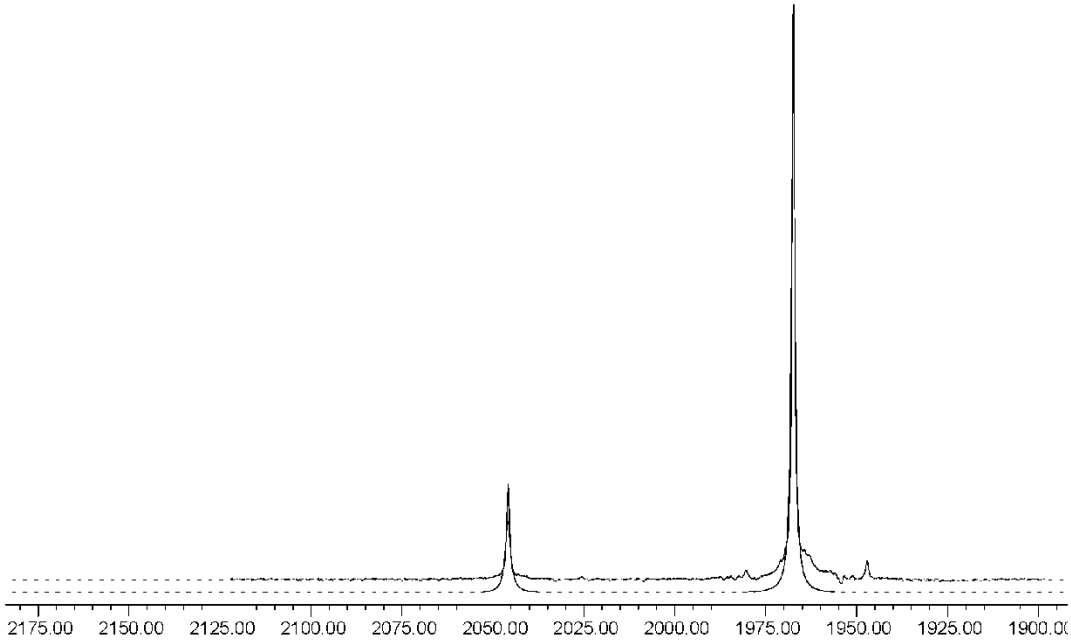

Figure S21. gNMR fitting for **1b/1c** exchange at -15 °C with 1.3 M DBU and 15.4 M CD_3CN.

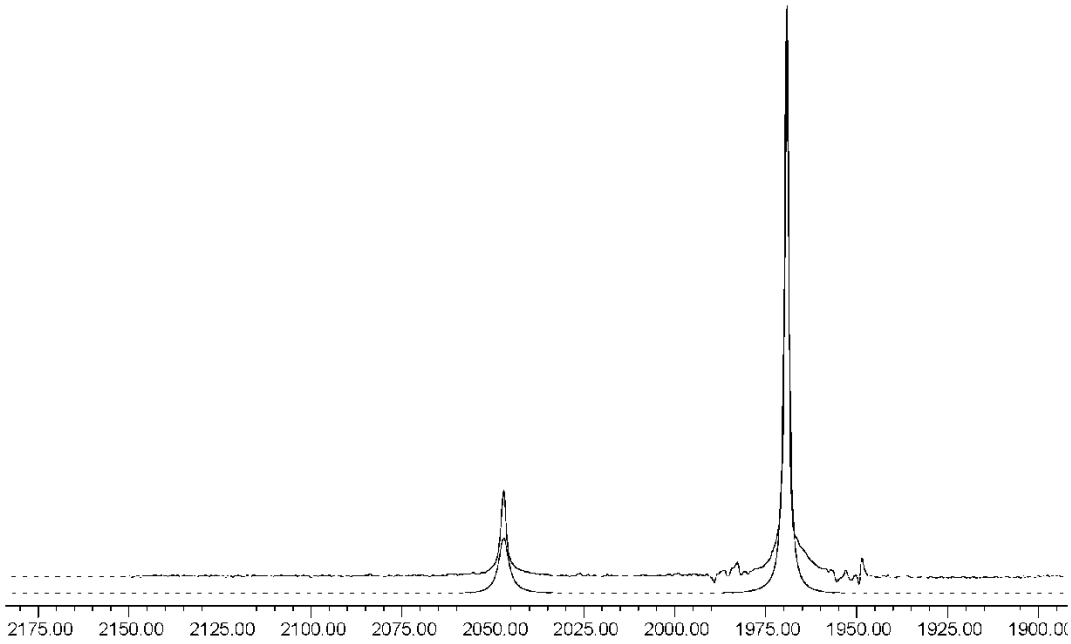

Figure S22. gNMR fitting for **1b/1c** exchange at -5 °C with 1.3 M DBU and 15.4 M CD_3CN.

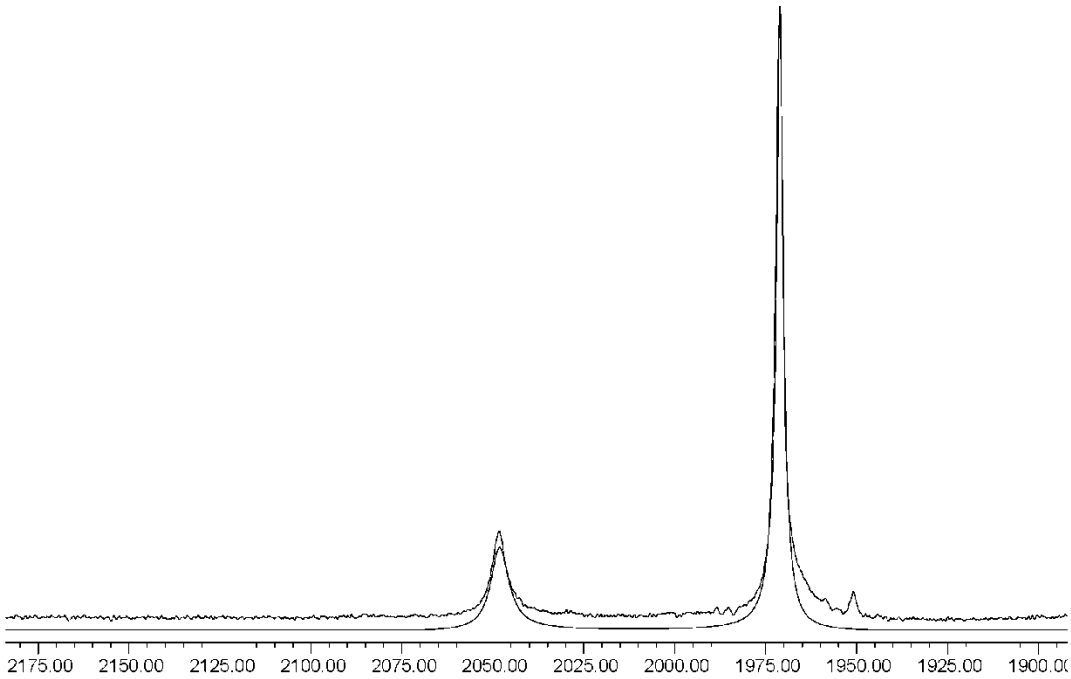

Figure S23. gNMR fitting for **1b/1c** exchange at 5 °C with 1.3 M DBU and 15.4 M CD_3CN.

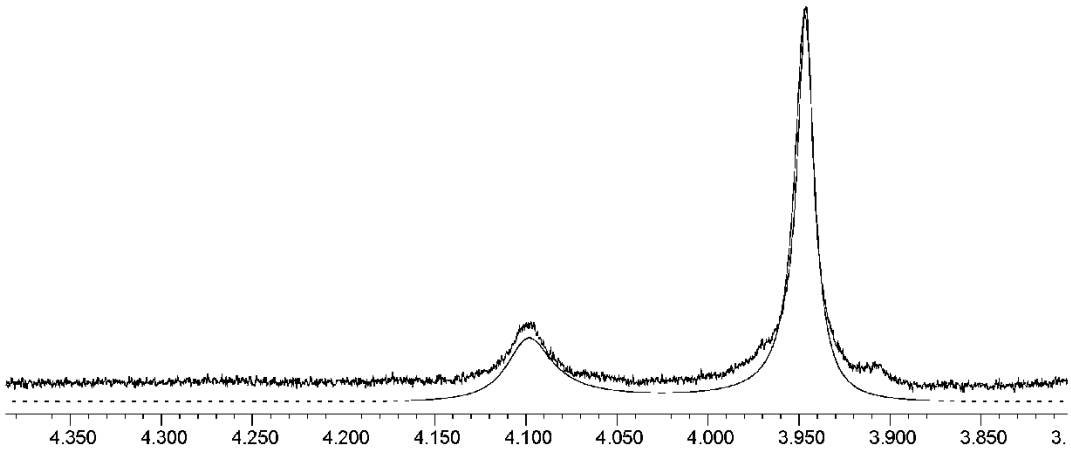

Figure S24. gNMR fitting for **1b/1c** exchange at 15 °C with 1.3 M DBU and 15.4 M CD_3CN.

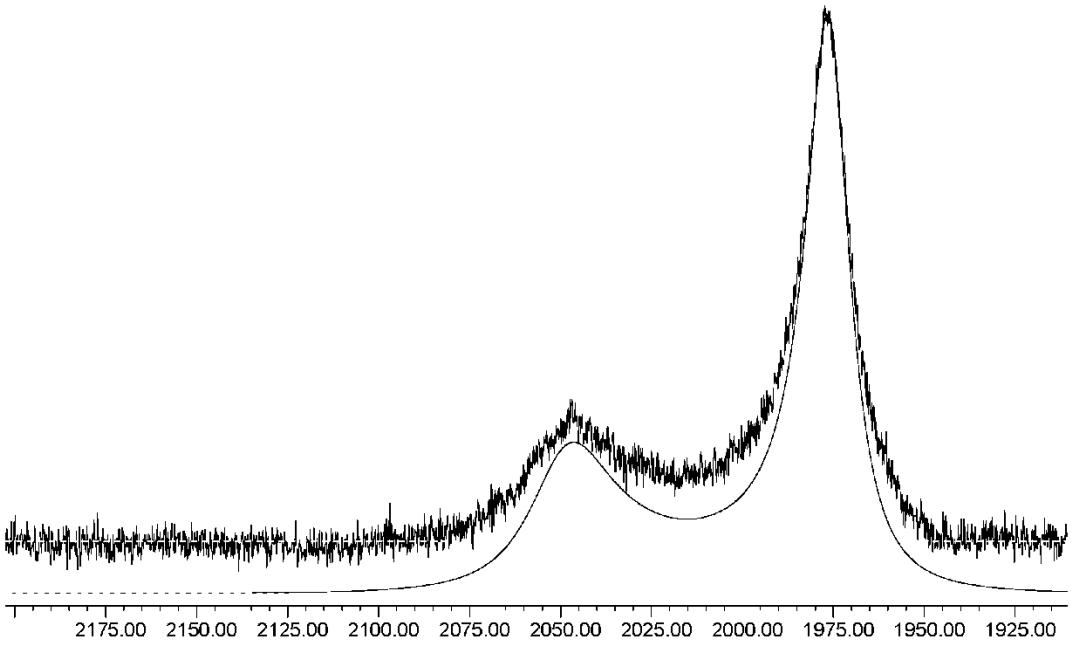

Figure S25. gNMR fitting for **1b/1c** exchange at 25 °C with 1.3 M DBU and 15.4 M CD_3CN.

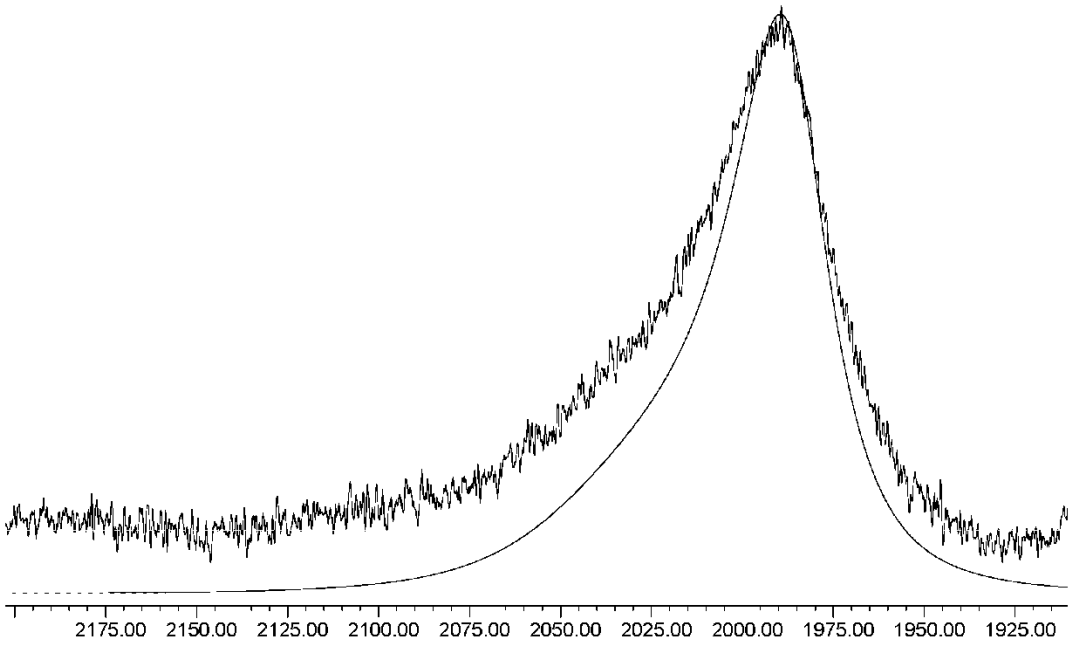

Figure S26. gNMR fitting for **1b/1c** exchange at 35 °C with 1.3 M DBU and 15.4 M CD_3CN.

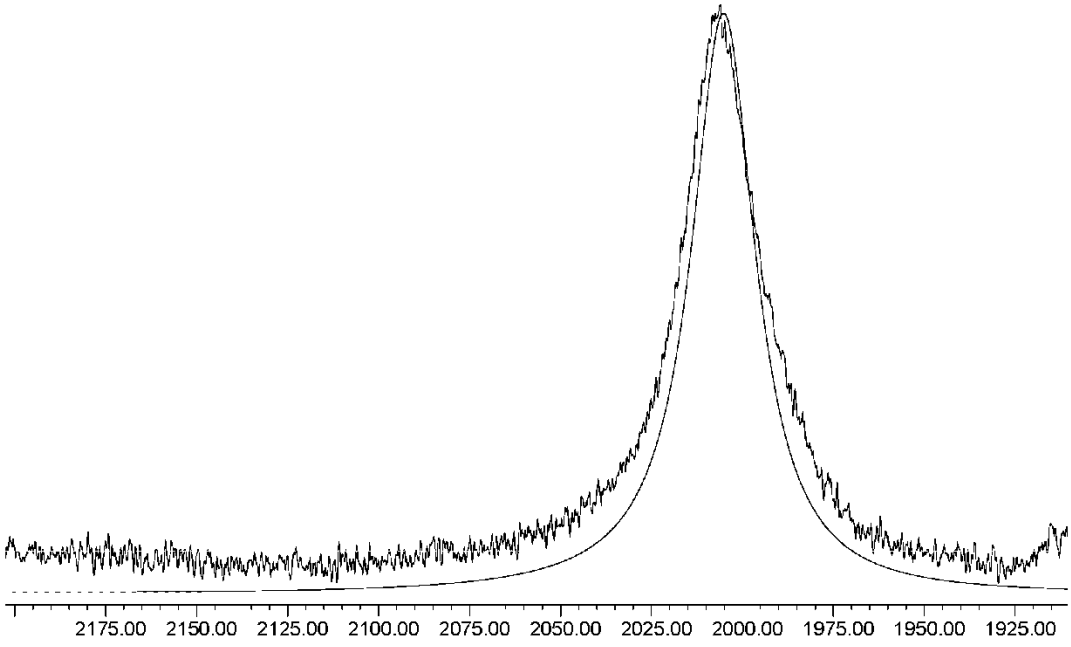

Figure S27. gNMR fitting for **1b/1c** exchange at 45 °C with 1.3 M DBU and 15.4 M CD_3CN.

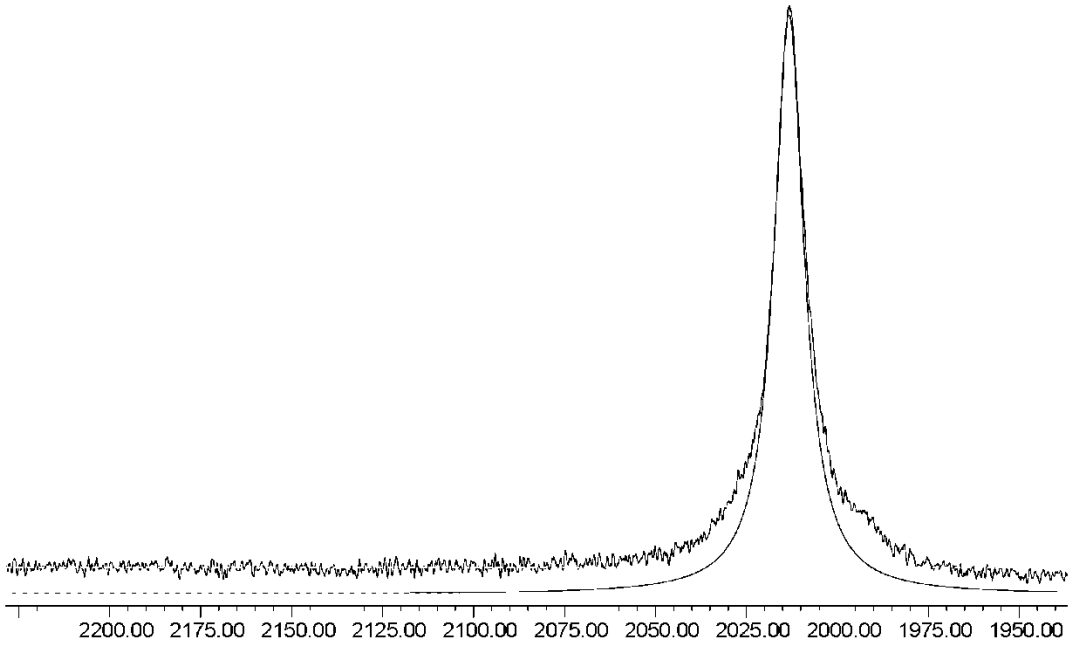

Figure S28. gNMR fitting for **1b/1c** exchange at 55 °C with 1.3 M DBU and 15.4 M CD_3CN.

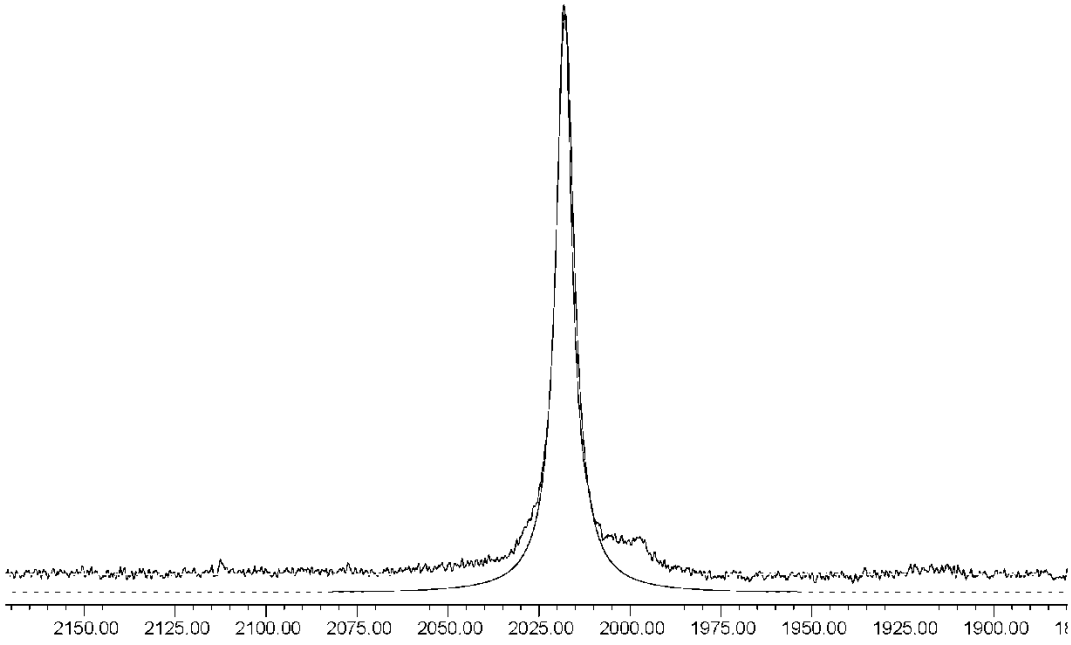

Figure S29. gNMR fitting for **1b/1c** exchange at 65 °C with 1.3 M DBU and 15.4 M CD_3CN.

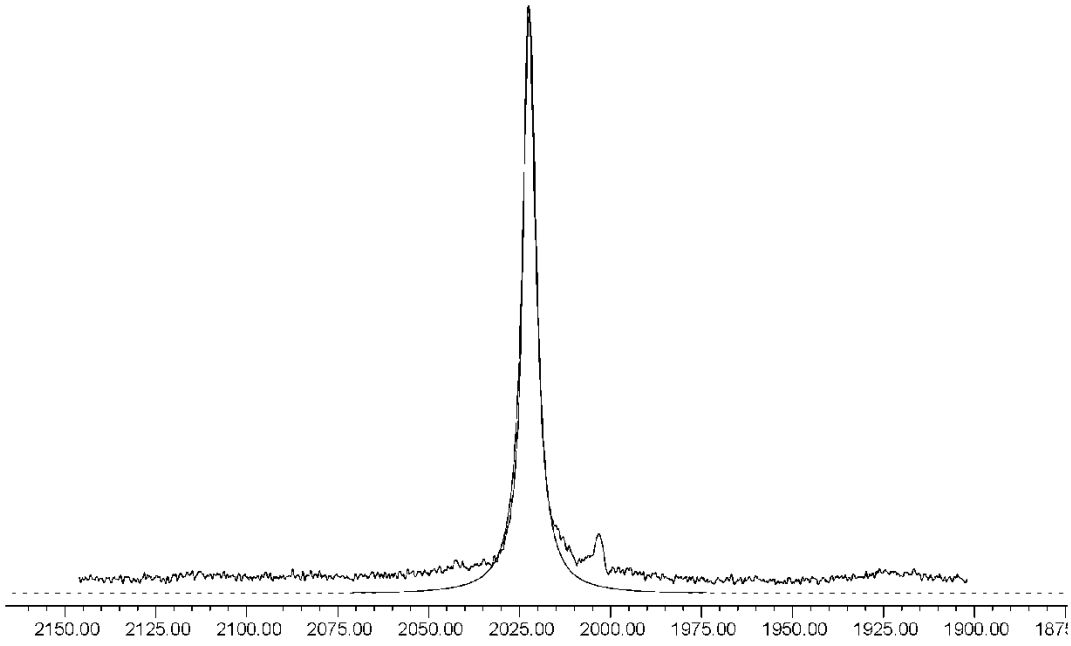

Figure S30. gNMR fitting for **1b/1c** exchange at 75 °C with 1.3 M DBU and 15.4 M CD_3CN.

Table S2. Observed exchange rate for K_2 determined from linewidth analysis

Temp. (K)	Exchange rate (s^{-1})
258	0.68
268	1.5
278	4.1
288	13
298	29
308	80
318	210
328	460
338	800
348	1100

*Spectroscopic Characterization of **2b***

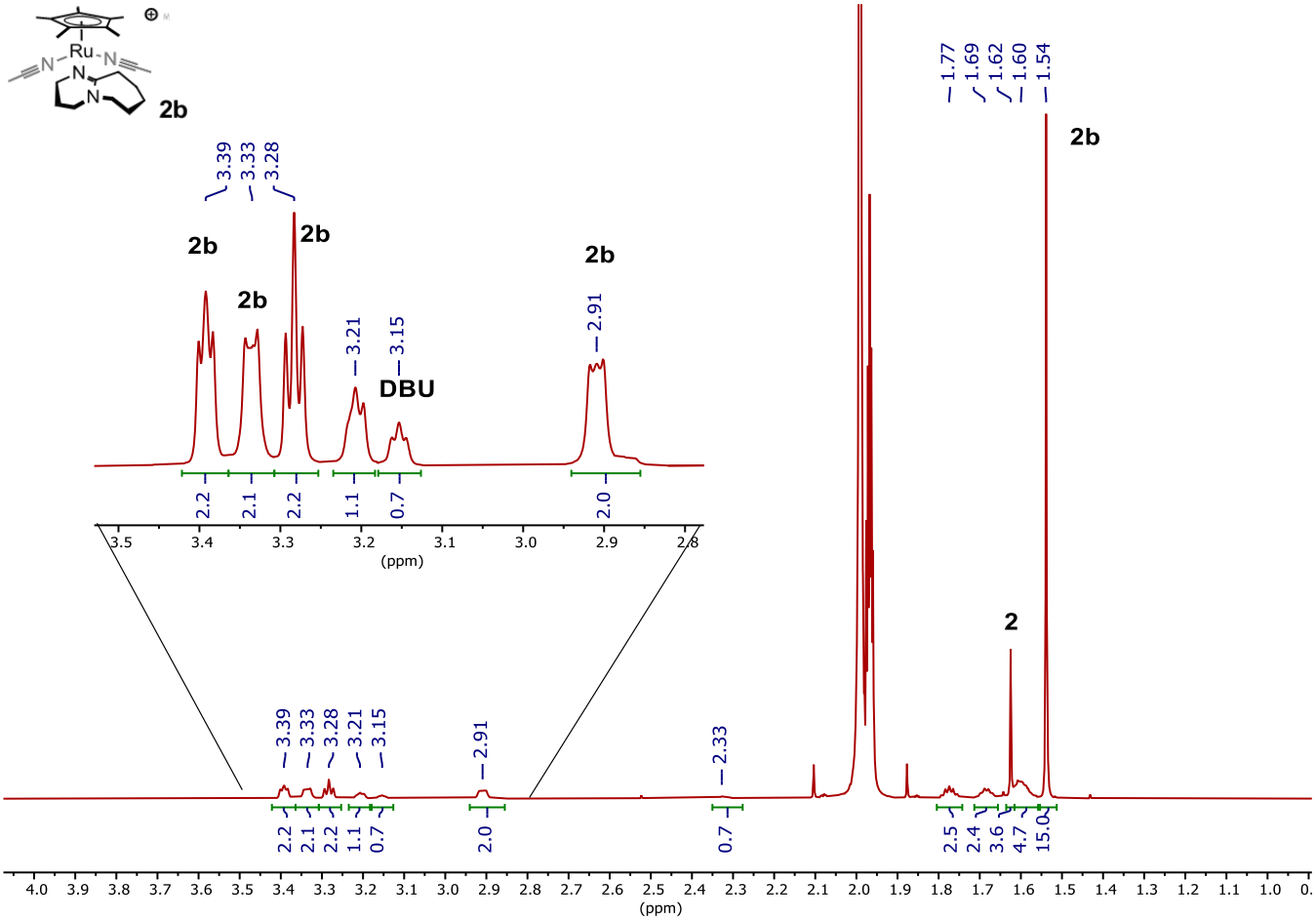

Figure S31. ^{1}H NMR spectra (600 MHz, CD_3CN, 298 K) of $[Cp^*Ru(MeCN)_3]^+$ (**2**, 25 mM) in the presence of DBU (25 mM).

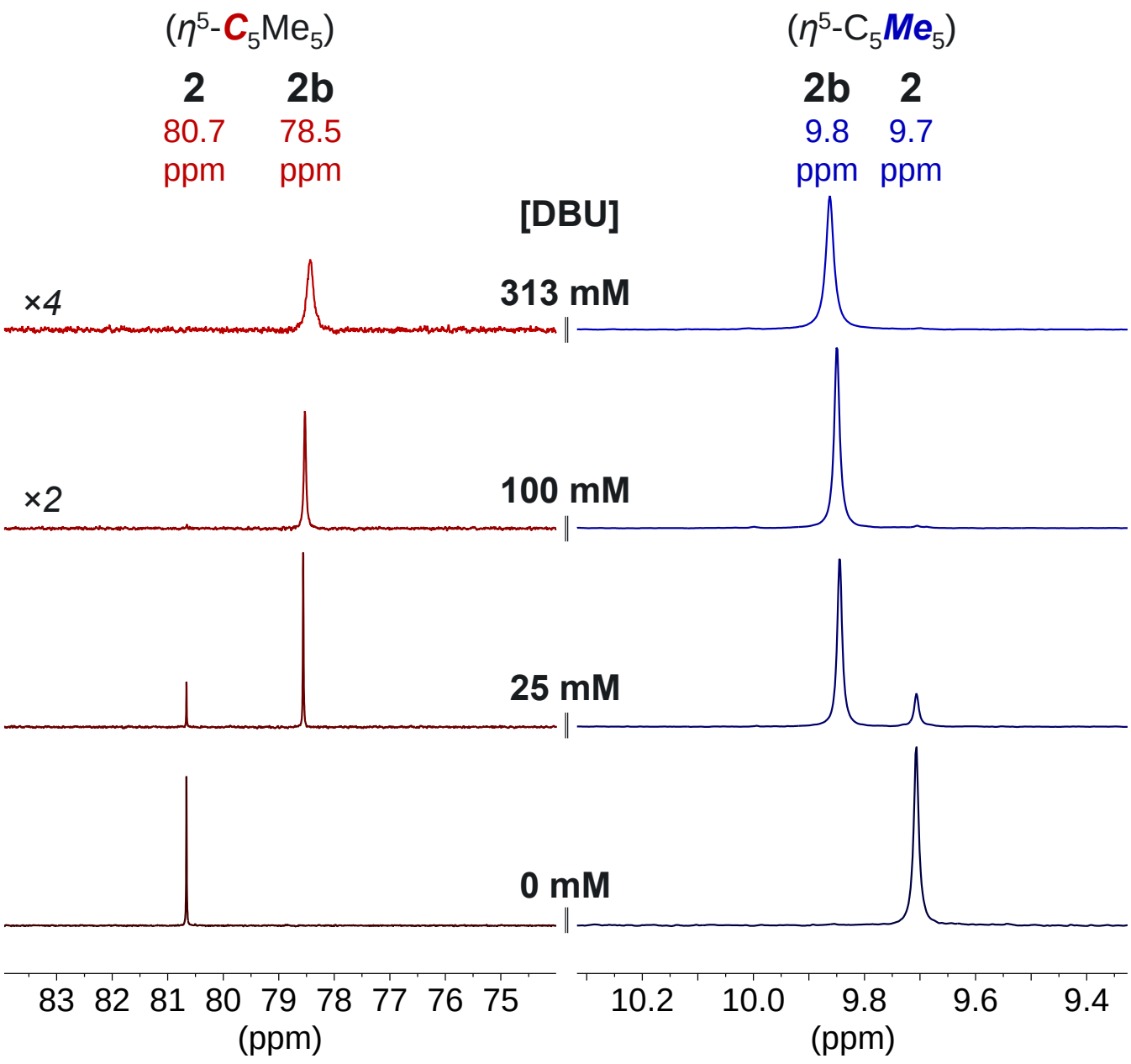

Figure S32. Partial $^{13}C\{^{1}H\}$ NMR spectra (151 MHz, CD_3CN, 25 °C) of **2** (25mM) with varying [DBU], focusing on the Cp* resonances. In this series of experiments, the CD_3CN concentration sequentially decreases from 19.15 M with no DBU (bottom spectrum) to 19.08 M, 18.86 M, and 18.25 M, respectively, as the DBU concentration increases from 25 mM to 313 mM.

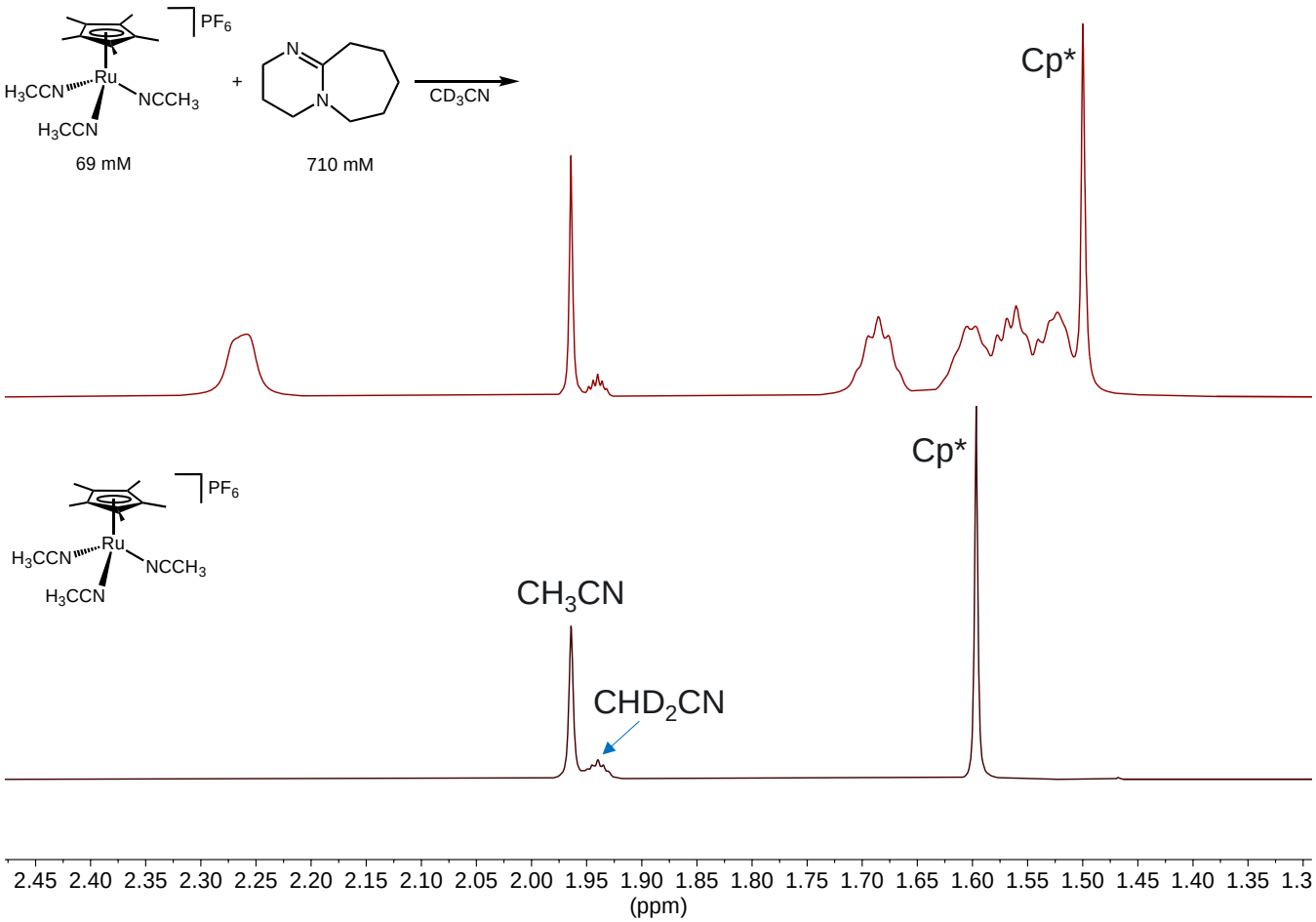

Figure S33. ^{1}H NMR spectra (600 MHz, CD_3CN, 298 K) of $[Cp^*Ru(MeCN)_3]^+$ (**2**, 69 mM) in the presence and absence of DBU (710 mM). The CD_3CN concentration decreases from 19.15 M with no DBU (bottom spectrum) to 17.1 M CD_3CN with 710 mM DBU.

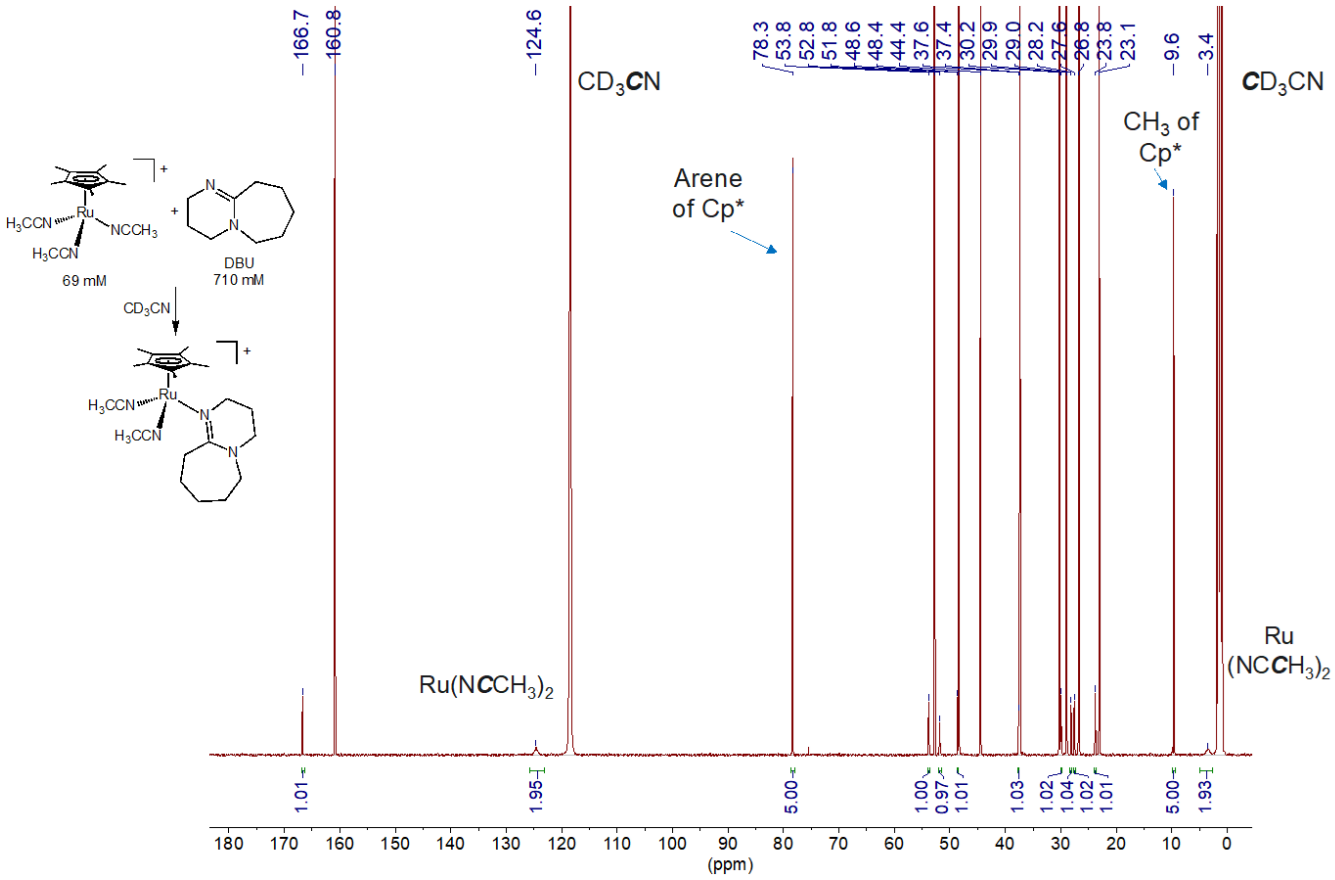

Figure S34. Low temperature inverse gated $^{13}C\{^{1}H\}$ NMR spectrum (151 MHz, CD_3CN, -30 °C) of $[Cp^*Ru(MeCN)_3]^+$ (**2**) with [DBU] = 710 mM and $[CD_3CN]$ = 17.1 M showing integration of 9 signals corresponding to Ru-bound DBU and two signals corresponding to Ru–$NCCH_3$. Integrations are consistent with the formation of $[CpRu(MeCN)_2(DBU)]^+$ under these conditions. See the next figure for a closer view of relevant signals.

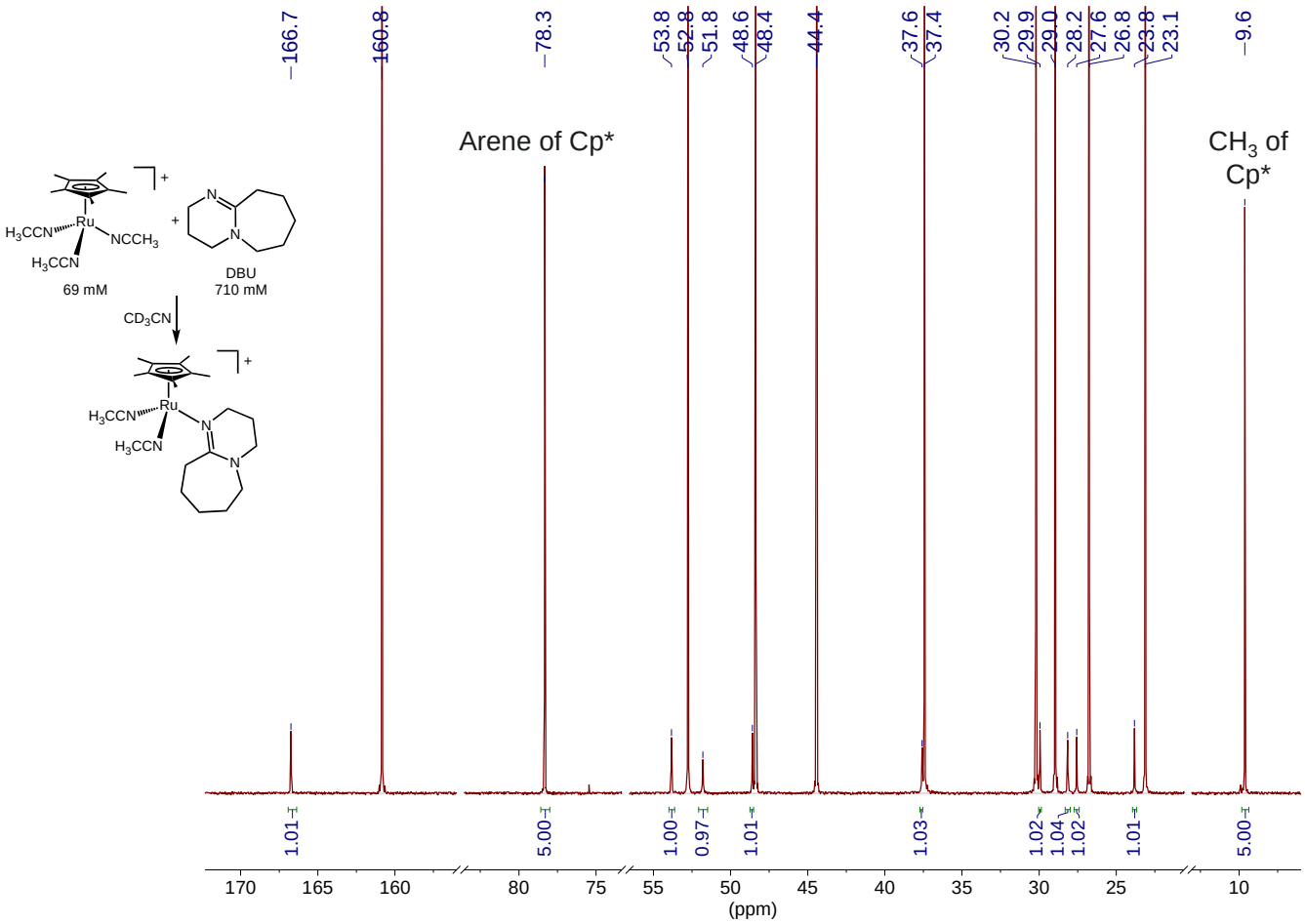

Figure S35. Partial reproduction of the previous figure focusing on the DBU and Cp* signals. Low temperature inverse gated $^{13}C\{^{1}H\}$ NMR spectrum (151 MHz, CD_3CN, 243 K) of $[Cp^*Ru(NCCH_3)_3]^+$ (**2**) with [DBU] = 710 mM and $[CD_3CN]$ = 17.1 M, consistent with the formation of $[Cp^*Ru(NCCH_3)_2(DBU)]^+$ (**2b**) under these conditions.

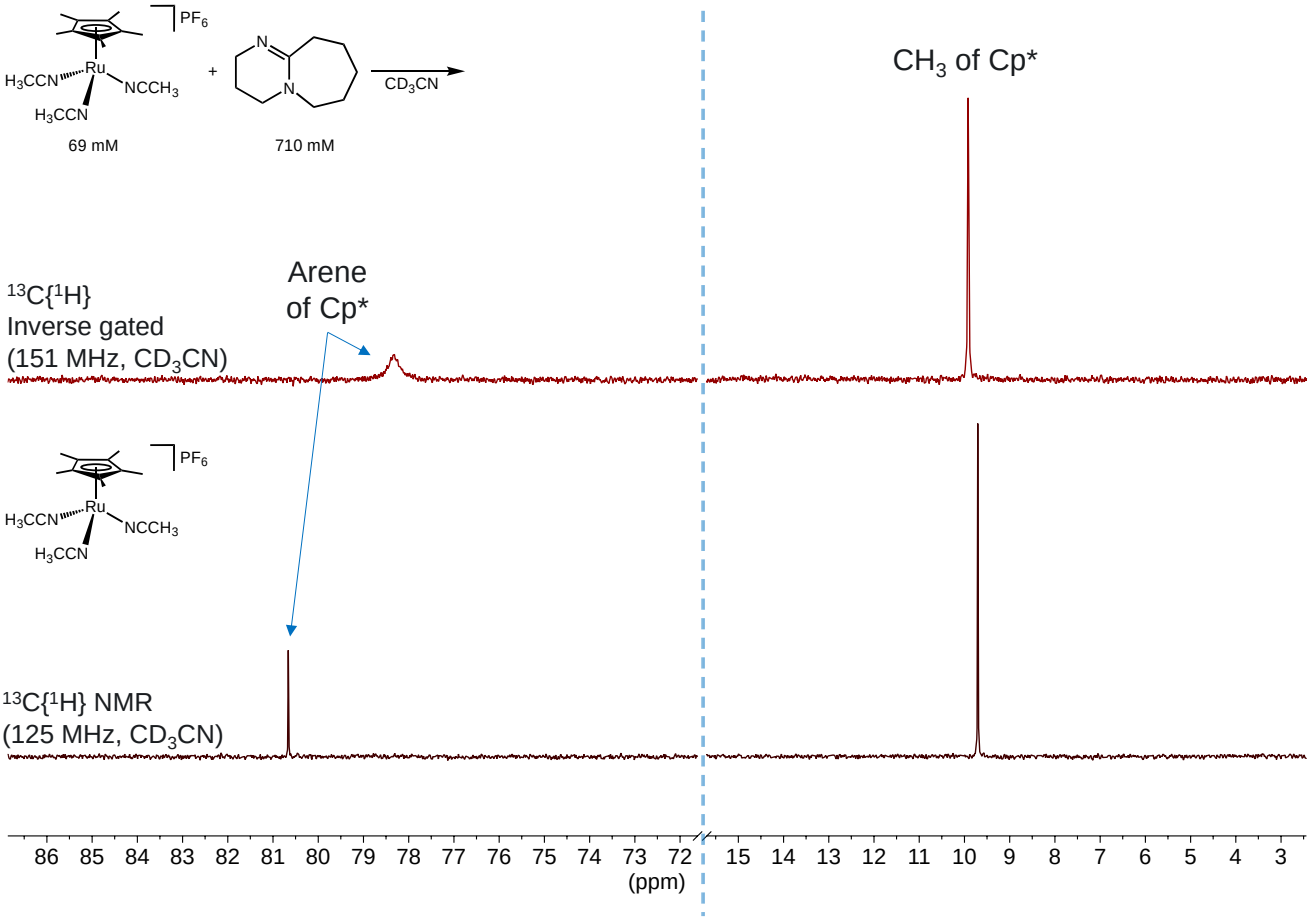

Figure S36. $^{13}C\{^{1}H\}$ NMR spectra of a CD_3CN solution of $[Cp^*Ru(NCCH_3)_3]^+$ (**2**) in the presence and absence of DBU (710 mM) focused on the Cp* resonances at 298 K. The CD_3CN concentration decreases from 19.15 M with no DBU (bottom spectrum) to 17.1 M CD_3CN with 710 mM DBU.

*Spectroscopic Characterization of **2c***

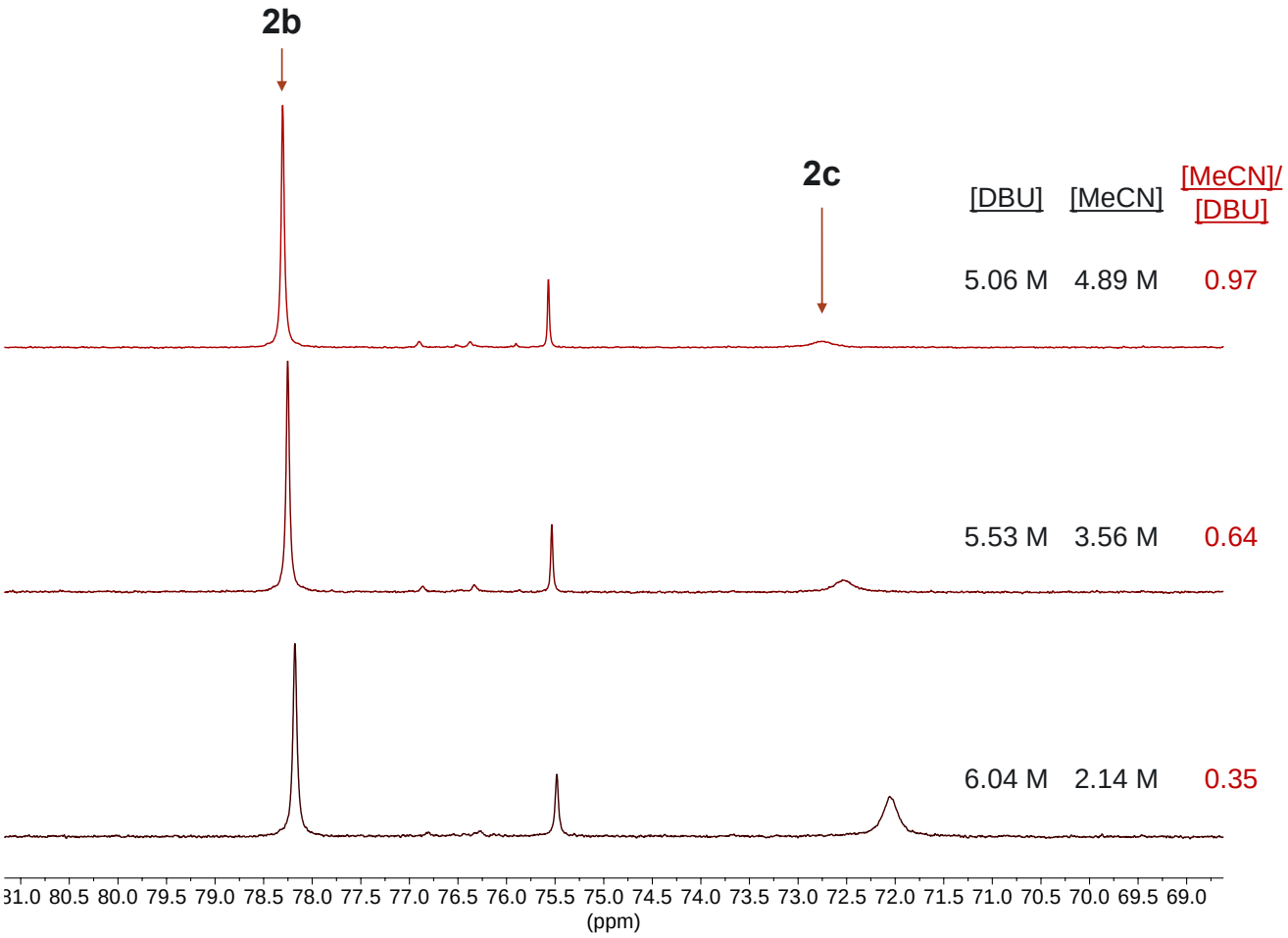

Figure S37. Comparison of low temperature $^{13}C\{^{1}H\}$ NMR spectra (151 MHz, CD_3CN, -25 °C) of $[Cp^*Ru(MeCN)_3]^+$ (**2**) with several high [DBU] (5-6 M) and low [MeCN] (4.9 - 2.1 M) showing the increase in the Cp* signals assigned to $[Cp^*Ru(MeCN)(DBU)_2]^+$ (**2c**) as [DBU] increased and [MeCN] decreased. Signal at 75.5 ppm is an unidentified impurity attributed to trace impurity in the DBU and comprises ~11% of the Cp* material with a 10:1 DBU:CD_3CN ratio by volume.

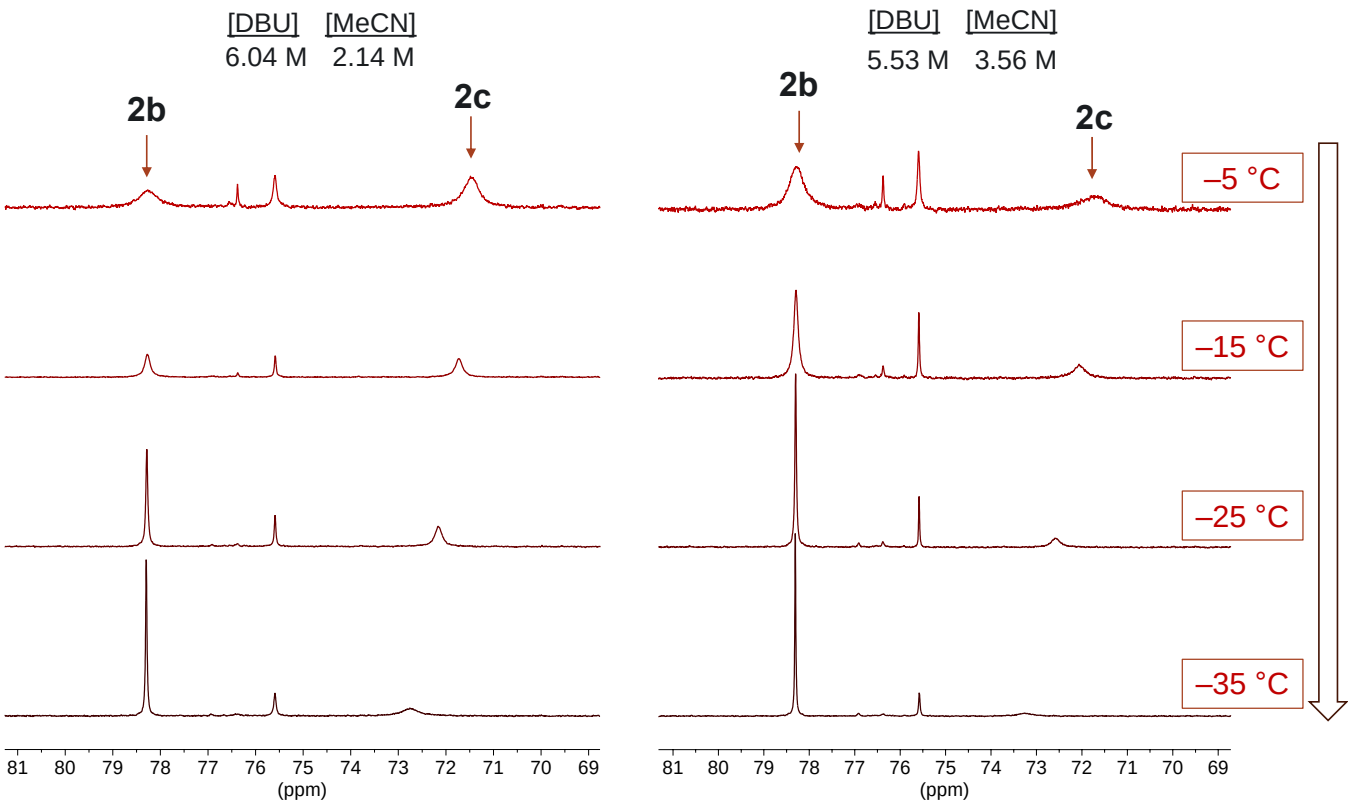

Figure S38. Comparison of low temperature $^{13}C\{^{1}H\}$ NMR spectra (151 MHz, CD_3CN) of $[Cp^*Ru(NCCH_3)_3]^+$ (**2**) with two high [DBU]/low [MeCN] showing the increase in the Cp* signals assigned to $[Cp^*Ru(MeCN)(DBU)_2]^+$ (**2c**) as the temperature is raised. Signal at 75.5 ppm is an unidentified impurity attributed to trace impurity in the DBU, comprises ~11% of the Cp* material and its relative integration does not change with temperature. Spectra at warmer temperatures are magnified to show peak broadening and changing peak areas. These spectra were used to calculate K_2 through integration of the resonances for **2b** and **2c**.

*X-ray Crystallographic Data for **2b***

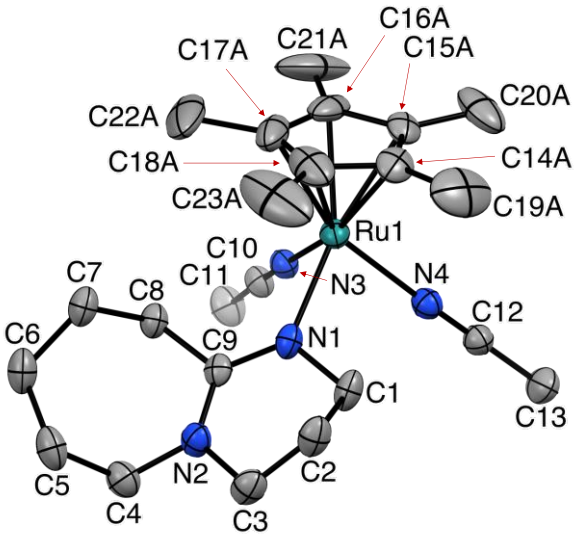

Figure S39. Cationic fragment of the solid-state structure of [Cp*Ru(DBU)($NCCH_3$)$_2$][PF_6] (**2b**) showing the full atom numbering. Thermal ellipsoids are displayed at 50% probability. Only one of the disorded Cp* positions is shown. PF_6^- anion, cocrystallized Et_2O, and hydrogen atoms are omitted.

Table S3. Crystal data and structure refinement for [Cp*Ru(DBU)(NCCH$_3$)$_2$][PF$_6$] (2b).

CCDC Deposition Number	**2329534**
Empirical formula	$C_{27}H_{47}F_6N_4OPRu$
Formula weight	689.72
Temperature/K	100
Crystal system	monoclinic
Space group	P2/n
a/Å	12.1425(7)
b/Å	10.9767(6)
c/Å	24.5384(13)
α/°	90
β/°	99.738(2)
γ/°	90
Volume/Å^3	3223.5(3)
Z	4
ρ_{calc}g/cm^3	1.421
μ/mm^{-1}	0.597
F(000)	1432
Crystal size/mm^3	0.219 × 0.159 × 0.112
Radiation	MoKα (λ = 0.71073)
2Θ range for data collection/°	4.044 to 55.904
Index ranges	-15 ≤ h ≤ 15, -14 ≤ k ≤ 14, -32 ≤ l ≤ 30
Reflections collected	71055
Independent reflections	7710 [R_{int} = 0.0522, R_{sigma} = 0.0290]
Data/restraints/parameters	7710/166/471
Goodness-of-fit on F^2	1.191
Final R indexes [I>=2σ (I)]	R_1 = 0.0570, wR_2 = 0.1237
Final R indexes [all data]	R_1 = 0.0738, wR_2 = 0.1348
Largest diff. peak/hole / e Å^{-3}	1.51/-0.91

Table S4. Selected Bond Lengths for [Cp*Ru(DBU)(NCCH$_3$)$_2$][PF$_6$] (2b).

Atom	Atom	Length/Å	Atom	Atom	Length/Å
Ru1	N3	2.096(3)	C17B	C18B	1.39(2)
Ru1	N4	2.097(3)	C17B	C22B	1.54(2)
Ru1	C14A	2.138(8)	C18A	C23A	1.493(16)
Ru1	C14B	2.122(17)	C18B	C23B	1.488(18)
Ru1	C15A	2.169(8)	N1	C1	1.473(5)
Ru1	C15B	2.111(13)	N1	C9	1.311(5)
Ru1	C16A	2.171(9)	N2	C3	1.479(5)
Ru1	C16B	2.164(17)	N2	C4	1.463(5)
Ru1	C17A	2.136(10)	N2	C9	1.347(5)
Ru1	C17B	2.166(16)	C1	C2	1.526(6)
Ru1	C18A	2.133(11)	C2	C3	1.511(6)
Ru1	C18B	2.135(14)	C4	C5	1.525(6)
Ru1	N1	2.184(3)	C5	C6	1.525(7)
N3	C10	1.140(5)	C6	C7	1.518(6)
N4	C12	1.146(5)	C7	C8	1.541(5)
C10	C11	1.462(6)	C8	C9	1.522(5)
C12	C13	1.452(6)			
C14A	C15A	1.426(14)			
C14A	C18A	1.456(15)			
C14A	C19A	1.493(13)			
C14B	C15B	1.41(2)			
C14B	C18B	1.45(2)			
C14B	C19B	1.52(2)			
C15A	C16A	1.412(12)			
C15A	C20A	1.515(11)			
C15B	C16B	1.45(2)			
C15B	C20B	1.507(17)			
C16A	C17A	1.426(17)			
C16A	C21A	1.475(14)			
C16B	C17B	1.406(19)			
C16B	C21B	1.455(19)			
C17A	C18A	1.387(18)			
C17A	C22A	1.517(13)			

Table S5. Selected Bond Angles for [Cp*Ru(DBU)(NCCH$_3$)$_2$][PF$_6$] (2b).

Atom	Atom	Atom	Angle/˚	Atom	Atom	Atom	Angle/˚
N3	Ru1	N4	83.34(13)	C17A	C16A	Ru1	69.4(6)
N3	Ru1	C14A	158.9(4)	C17A	C16A	C21A	126.8(15)
N3	Ru1	C14B	141.6(8)	C21A	C16A	Ru1	126.0(7)
N3	Ru1	C15A	120.5(4)	C15B	C16B	Ru1	68.2(8)
N3	Ru1	C15B	105.6(6)	C15B	C16B	C21B	127.3(19)
N3	Ru1	C16A	96.4(3)	C17B	C16B	Ru1	71.1(10)
N3	Ru1	C16B	96.6(4)	C17B	C16B	C15B	105.2(14)
N3	Ru1	C17A	106.0(5)	C17B	C16B	C21B	127(2)
N3	Ru1	C17B	122.7(7)	C21B	C16B	Ru1	127.1(13)
N3	Ru1	C18A	141.1(6)	C16A	C17A	Ru1	72.0(6)
N3	Ru1	C18B	160.3(7)	C16A	C17A	C22A	126.5(19)
N3	Ru1	N1	89.66(12)	C18A	C17A	Ru1	70.9(7)
N4	Ru1	C14A	99.9(3)	C18A	C17A	C16A	108.9(10)
N4	Ru1	C14B	93.7(5)	C18A	C17A	C22A	124(2)
N4	Ru1	C15A	95.3(3)	C22A	C17A	Ru1	129.1(7)
N4	Ru1	C15B	107.5(6)	C16B	C17B	Ru1	71.0(10)
N4	Ru1	C16A	124.0(5)	C16B	C17B	C22B	126(2)
N4	Ru1	C16B	145.9(6)	C18B	C17B	Ru1	69.9(10)
N4	Ru1	C17A	159.9(4)	C18B	C17B	C16B	112.8(15)
N4	Ru1	C17B	153.5(7)	C18B	C17B	C22B	121(2)
N4	Ru1	C18A	135.5(6)	C22B	C17B	Ru1	126.9(13)
N4	Ru1	C18B	116.0(7)	C14A	C18A	Ru1	70.3(6)
N4	Ru1	N1	85.31(12)	C14A	C18A	C23A	125(2)
C14A	Ru1	C15A	38.7(4)	C17A	C18A	Ru1	71.2(7)
C14A	Ru1	C16A	64.4(4)	C17A	C18A	C14A	107.8(11)
C14A	Ru1	N1	111.3(4)	C17A	C18A	C23A	127.5(19)
C14B	Ru1	C16B	65.4(6)	C23A	C18A	Ru1	124.8(8)
C14B	Ru1	C17B	63.5(7)	C14B	C18B	Ru1	69.6(9)
C14B	Ru1	C18B	39.9(6)	C14B	C18B	C23B	126(2)
C14B	Ru1	N1	128.3(8)	C17B	C18B	Ru1	72.4(10)
C15A	Ru1	C16A	38.0(3)	C17B	C18B	C14B	105.1(14)
C15A	Ru1	N1	149.7(4)	C17B	C18B	C23B	129(2)
C15B	Ru1	C14B	39.0(6)	C23B	C18B	Ru1	128.9(11)
C15B	Ru1	C16B	39.5(6)	C1	N1	Ru1	114.1(2)
C15B	Ru1	C17B	64.0(6)	C9	N1	Ru1	129.4(3)
C15B	Ru1	C18B	66.5(5)	C9	N1	C1	116.4(3)
C15B	Ru1	N1	160.9(4)	C4	N2	C3	114.2(3)
C16A	Ru1	N1	150.6(5)	C9	N2	C3	121.6(3)
C16B	Ru1	C17B	37.9(5)	C9	N2	C4	123.9(4)
C16B	Ru1	N1	128.8(6)	N1	C1	C2	111.4(3)
C17A	Ru1	C14A	65.0(4)	C3	C2	C1	108.6(4)
C17A	Ru1	C15A	64.5(4)	N2	C3	C2	109.8(4)
C17A	Ru1	C16A	38.7(5)	N2	C4	C5	114.1(4)

Table S5. Selected Bond Angles for [Cp*Ru(DBU)(NCCH$_3$)$_2$][PF$_6$] (2b).

Atom	Atom	Atom	Angle/˚	Atom	Atom	Atom	Angle/˚
C17A	Ru1	N1	112.0(6)	C6	C5	C4	112.8(4)
C17B	Ru1	N1	98.2(5)	C7	C6	C5	114.1(4)
C18A	Ru1	C14A	39.8(4)	C6	C7	C8	115.4(4)
C18A	Ru1	C15A	65.2(4)	C9	C8	C7	114.1(3)
C18A	Ru1	C16A	64.3(5)	N1	C9	N2	125.4(4)
C18A	Ru1	C17A	37.9(5)	N1	C9	C8	118.4(4)
C18A	Ru1	N1	93.4(4)	N2	C9	C8	116.2(3)
C18B	Ru1	C16B	65.6(6)				
C18B	Ru1	C17B	37.7(6)				
C18B	Ru1	N1	95.3(4)				
C10	N3	Ru1	177.4(3)				
C12	N4	Ru1	178.0(3)				
N3	C10	C11	178.9(5)				
N4	C12	C13	178.8(5)				
C15A	C14A	Ru1	71.8(5)				
C15A	C14A	C18A	107.0(10)				
C15A	C14A	C19A	125.1(14)				
C18A	C14A	Ru1	69.9(6)				
C18A	C14A	C19A	127.8(18)				
C19A	C14A	Ru1	125.9(7)				
C15B	C14B	Ru1	70.1(9)				
C15B	C14B	C18B	108.5(13)				
C15B	C14B	C19B	125(2)				
C18B	C14B	Ru1	70.5(9)				
C18B	C14B	C19B	126(2)				
C19B	C14B	Ru1	123.8(13)				
C14A	C15A	Ru1	69.5(5)				
C14A	C15A	C20A	124.7(13)				
C16A	C15A	Ru1	71.1(5)				
C16A	C15A	C14A	108.0(10)				
C16A	C15A	C20A	127.2(14)				
C20A	C15A	Ru1	127.3(6)				
C14B	C15B	Ru1	70.9(9)				
C14B	C15B	C16B	108.2(12)				
C14B	C15B	C20B	125(2)				
C16B	C15B	Ru1	72.2(9)				
C16B	C15B	C20B	126(2)				
C20B	C15B	Ru1	131.1(11)				
C15A	C16A	Ru1	70.9(5)				
C15A	C16A	C17A	108.2(10)				
C15A	C16A	C21A	125.0(16)				

Table S6. Atomic Occupancy for [Cp*Ru(DBU)(NCCH$_3$)$_2$][PF$_6$] (2b).

Atom	Occupancy	Atom	Occupancy	Atom	Occupancy
C14A	0.655(8)	C14B	0.345(8)	C15A	0.655(8)
C15B	0.345(8)	C16A	0.655(8)	C16B	0.345(8)
C17A	0.655(8)	C17B	0.345(8)	C18A	0.655(8)
C18B	0.345(8)	C19A	0.655(8)	H19A	0.655(8)
H19B	0.655(8)	H19C	0.655(8)	C19B	0.345(8)
H19D	0.345(8)	H19E	0.345(8)	H19F	0.345(8)
C20A	0.655(8)	H20A	0.655(8)	H20B	0.655(8)
H20C	0.655(8)	C20B	0.345(8)	H20D	0.345(8)
H20E	0.345(8)	H20F	0.345(8)	C21A	0.655(8)
H21A	0.655(8)	H21B	0.655(8)	H21C	0.655(8)
C21B	0.345(8)	H21D	0.345(8)	H21E	0.345(8)
H21F	0.345(8)	C22A	0.655(8)	H22A	0.655(8)
H22B	0.655(8)	H22C	0.655(8)	C22B	0.345(8)
H22D	0.345(8)	H22E	0.345(8)	H22F	0.345(8)
C23A	0.655(8)	H23A	0.655(8)	H23B	0.655(8)
H23C	0.655(8)	C23B	0.345(8)	H23D	0.345(8)
H23E	0.345(8)	H23F	0.345(8)	F2A	0.549(15)
F2B	0.451(15)	F3A	0.549(15)	F3B	0.451(15)

DBU Binding Equilibria

DBU binding to **1** and **2** is accompanied by dissociation of an acetonitrile ligand, and thus the equilibrium depends on the relative molar ratio of DBU and MeCN solvent. The typical convention would be to exclude the concentration of solvent from the expression based on the assumption the solvent activity is constant due to the volume of the solutes being much lower than that of the solvent. However, this assumption is not valid for our studies due to the wide range of DBU concentrations employed. Therefore the equilibrium constants were expressed with explicit solvent (CD_3CN) and are hence unitless, as shown here for binding of the first DBU to **1**:

$$K_1 = \frac{[\mathbf{1b}][\mathrm{CD_3CN}]}{[\mathbf{1}][\mathrm{DBU}]} \qquad \text{(S1)}$$

Van 't Hoff plots were constructed over a temperature range in which the resonances for the Ru species are separated and well resolved due to a slow exchange, such that the relative concentrations of Ru species could be quantified by integration. For the equilibrium between **1b** and **1c**, the Van 't Hoff plots also include data at higher temperatures (35°C to 75°C) where the rate of exchange had accelerated enough that the two peaks had coalesced. For this temperature range, the concentrations of **1b** and **1c** were determined by the peak shift of the coalesced peak compared to the individual peaks if fully separated. To do this accurately, the theoretical positions of the two peaks at each temperature were extrapolated from a linear fit to the peak positions at -35°C to 10°C (**Figure S43**). The concentrations of each species were then calculated by Equations (S2) and (S3):

$$[\mathbf{1b}] = [\mathrm{Ru}_{tot}] * (\delta_{eq} - \delta_{1c}) \qquad \text{(S2)}$$

$$[\mathbf{1c}] = [\mathrm{Ru}_{tot}] * (\delta_{1b} - \delta_{eq}) \qquad \text{(S3)}$$

In Equations (S2)–(S3), δ_{1c} and δ_{1b} are the chemical shifts of the theoretical individual signals for Cp*H* in **1b** and **1c**, respectively, and δ_{eq} is the observed equilibrium chemical shift.

Table S7. Summary of thermodynamics for DBU binding.[a]

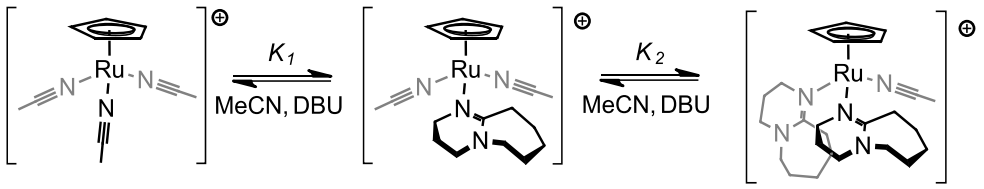

1 / 2 **1b / 2b** **1c / 2c**

Complex	K_1 (298 K)	$\Delta H°_1$ (kcal mol^{-1})	$\Delta S°_1$ (cal mol^{-1} K^{-1})	K_2 (298 K)	$\Delta H°_2$ (kcal mol^{-1})	$\Delta S°_2$ (cal mol^{-1} K^{-1})
1	1.2×10^5	−6.9 ± 0.6	0.2 ±1.0	66	−4.1 ± 0.1	−5.5 ± 0.2
2	1.8×10^4	−7.2 ± 0.3	−4.6 ± 0.8	0.9	5.1 ± 0.8	17 ± 3

[a] Uncertainties are listed at one standard deviation and are obtained from linear regression analysis of the Van 't Hoff plots in **Figure S40.**

As mentioned in the main text, the large differences in $\Delta H°_2$ and $\Delta S°_2$ suggest that the CH_3CN ligand of **2c** may be much more labile than in **1c** according to the following equilibrium reaction:

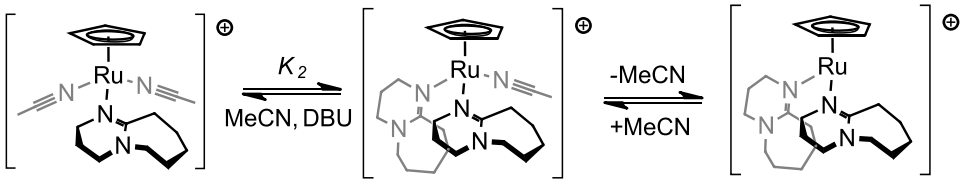

1b / 2b **1c / 2c** **1c' / 2c'**

Dissociation of the CH_3CN ligand in **1c** / **2c** would be expected to be: (a) endothermic ($\Delta H° > 0$) due to the loss of a Ru−N bond, and (b) entropically favored ($\Delta S° > 0$) due to one molecule (**1c**/**2c**) transforming to two molecules (**1c′**/**2c′** and MeCN). These thermodynamic characteristics are observed for K_2, suggesting that **2c** may exist primarily as a **2c′**. However, this could not be confirmed by $^{13}C\{^1H\}$ NMR spectroscopy since only the Cp* resonances were observed under the conditions leading to significant conversion to **2c**.

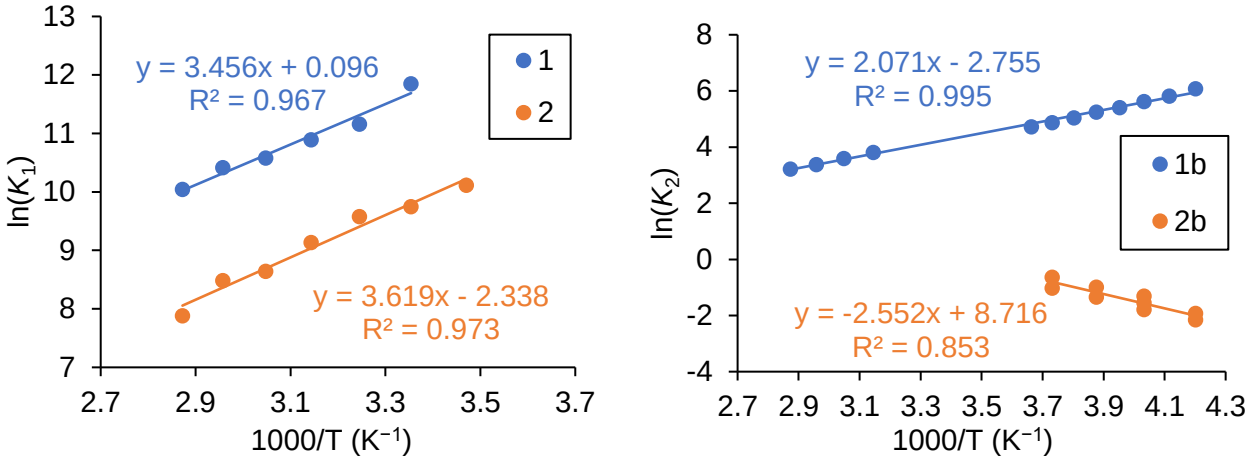

Figure S40. Van 't Hoff plots for binding of the first DBU (left) and the second DBU (right).

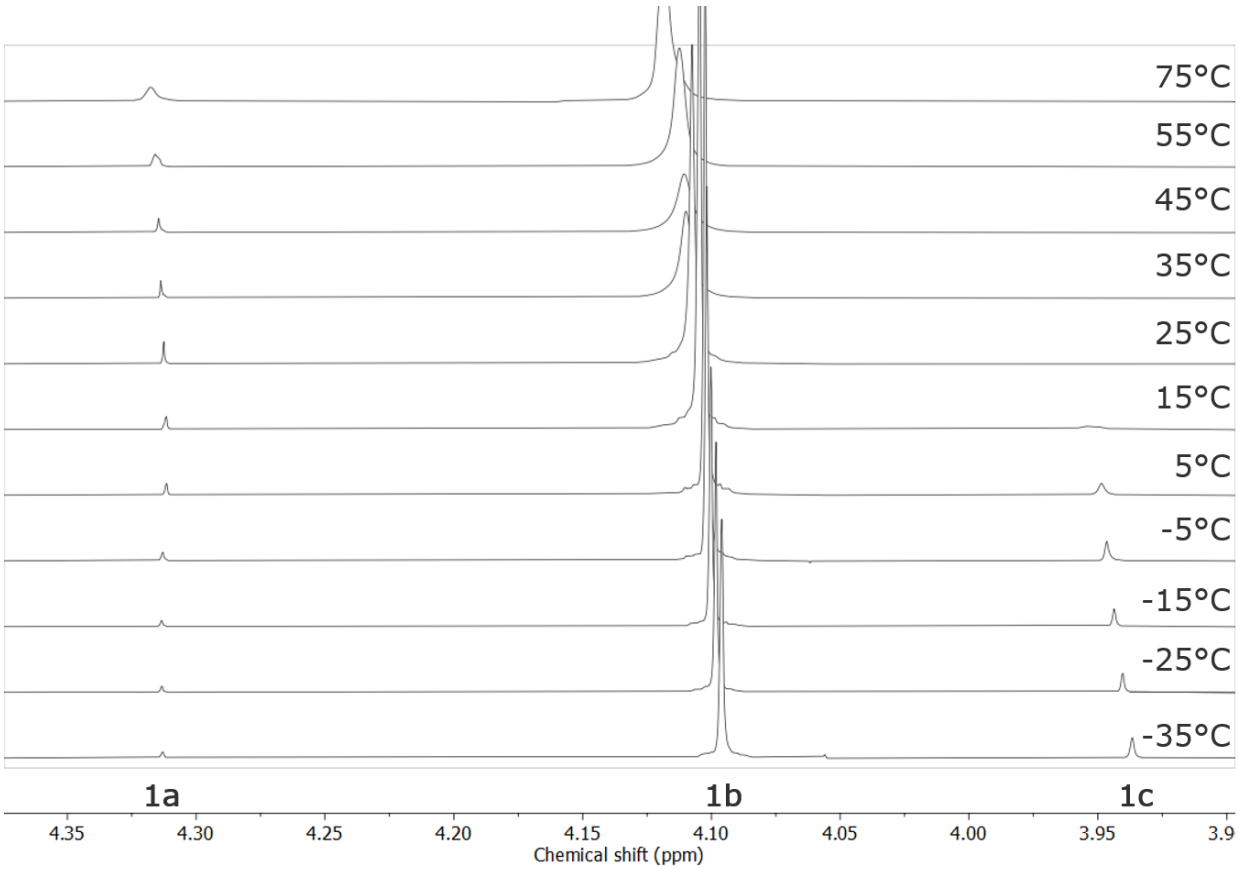

Figure S41. ^{1}H NMR spectra (500 MHz, CD_3CN) of **1** (57 mM) and DBU (65 mM) from -35 °C to 75 °C. These spectra were used to calculate K_1 through integration of the resonances for **1a** and **1b**.

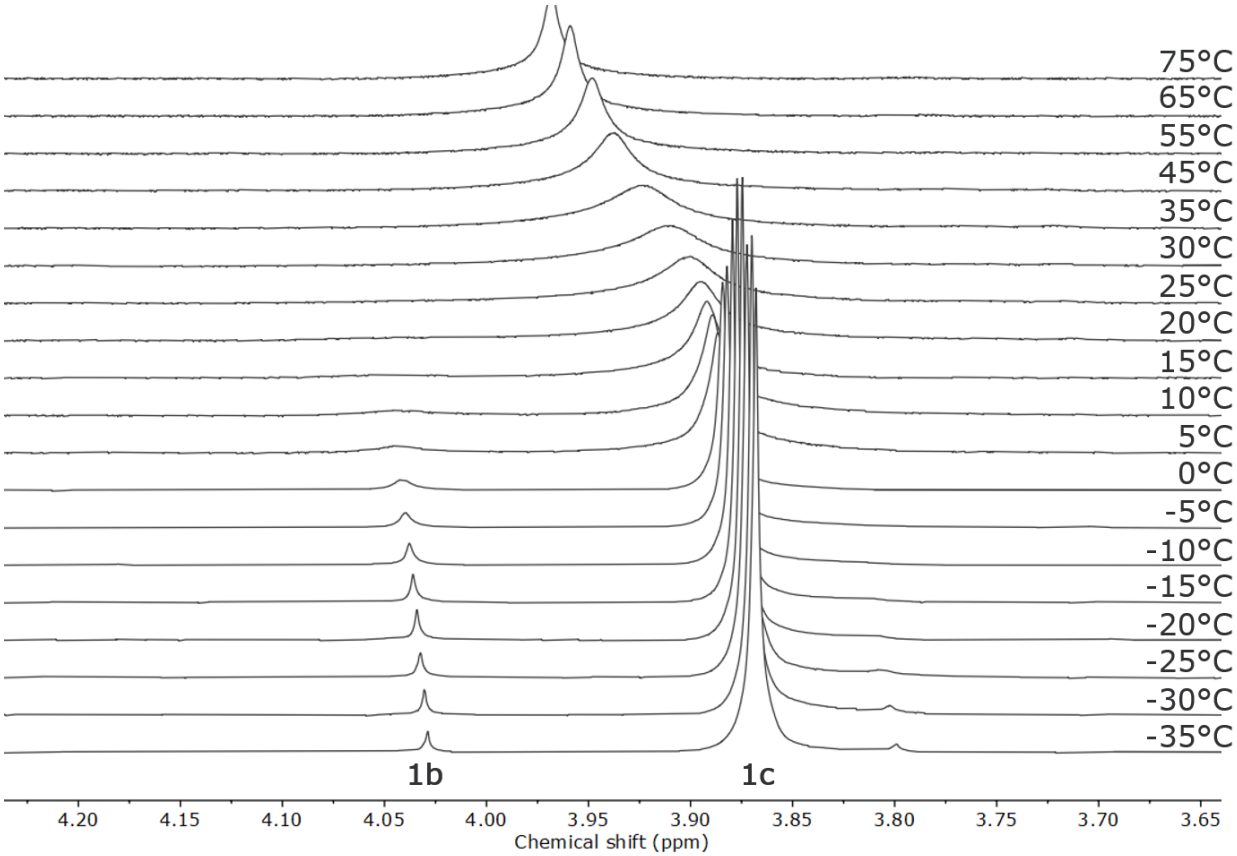

Figure S42. ^{1}H NMR spectra (500 MHz, CD_3CN) of **1** (39 mM) and DBU (1.3 M) from -35 °C to 75 °C. These spectra were used to calculate K_2 through integration of the resonances for **1b** and **1c** at low temp and by peak shift analysis at high temp.

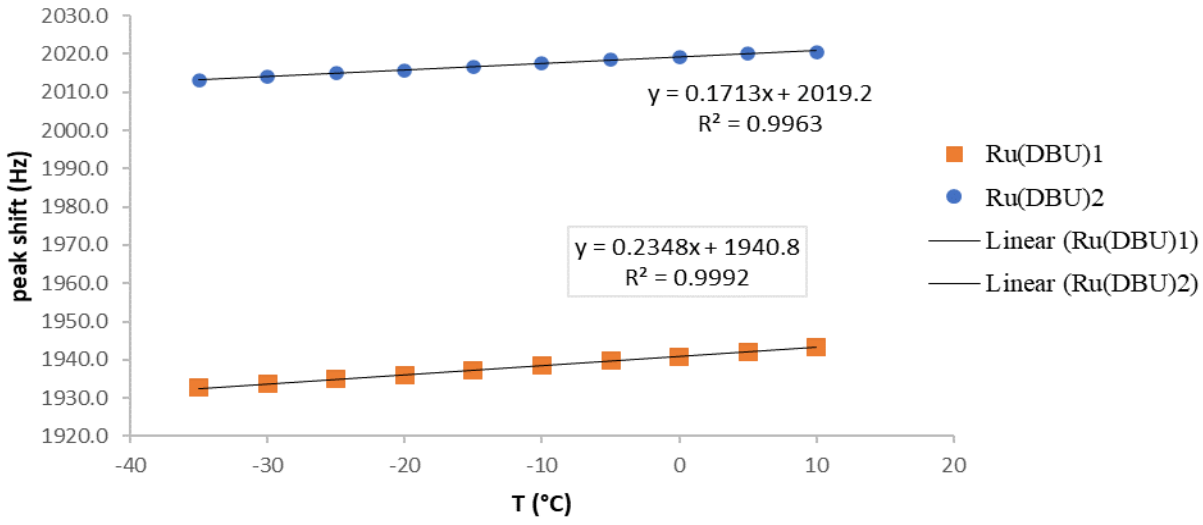

Figure S43. Temperature shift of Cp*H* resonance of **1b** and **1c** as a function of temperature.

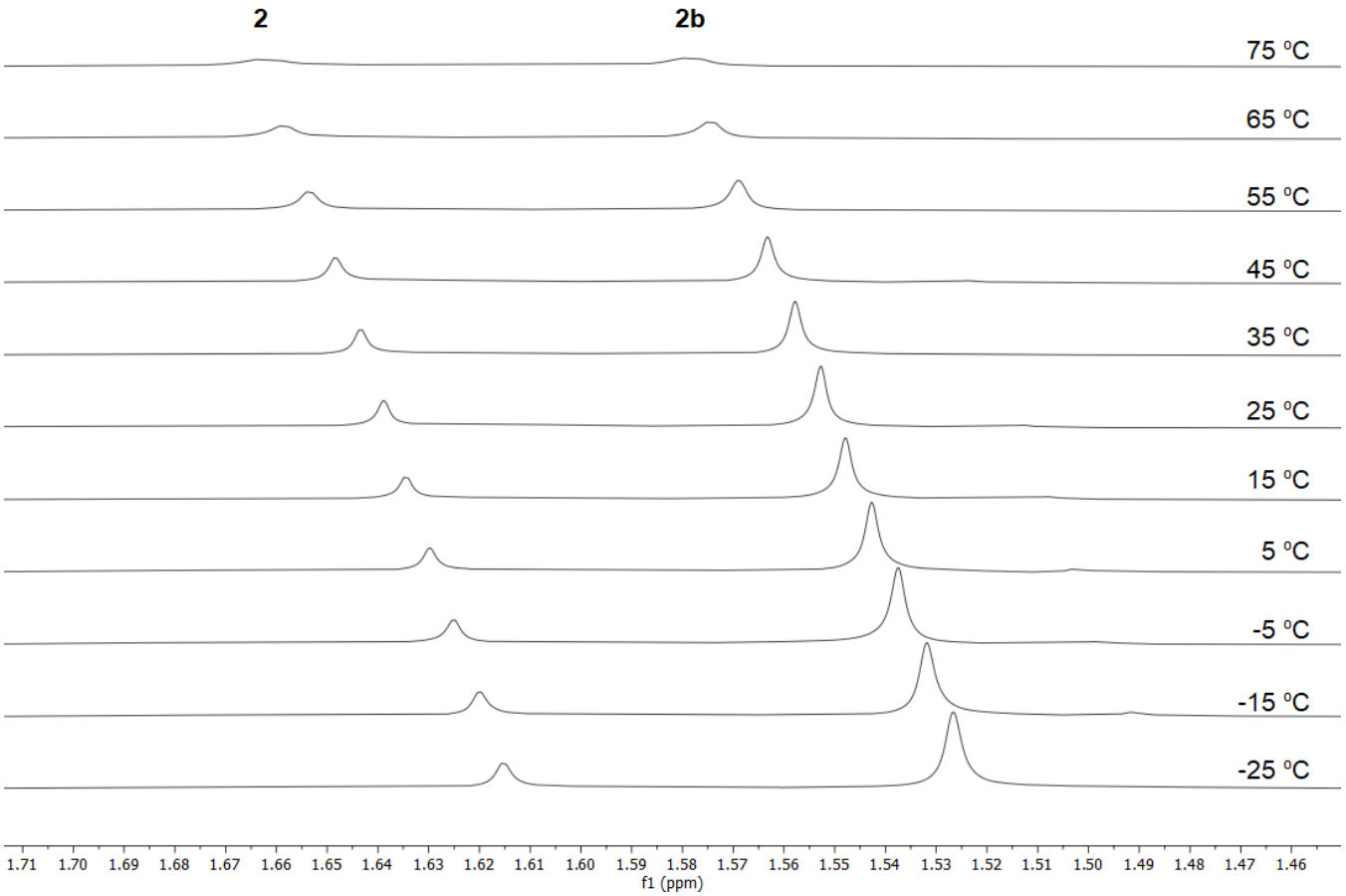

Figure S44. ^{1}H NMR spectra (500 MHz, CD_3CN) of **2** (17 mM) and DBU (15 mM) from -35 °C to 75 °C. These spectra were used to calculate K_1 through integration of the resonances for **2** and **2b**.

Temperature Dependence of a Ru(PNP) Catalyst

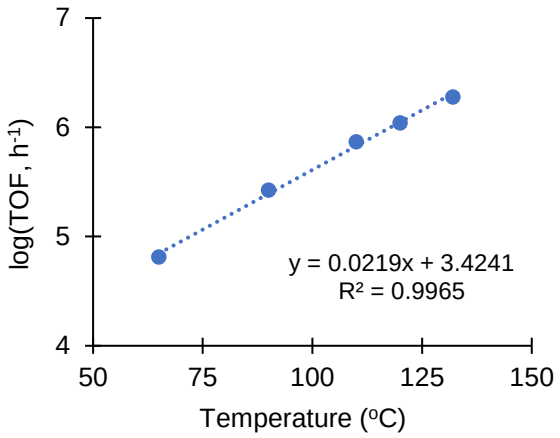

Figure S45. Previously reported temperature-dependent TOF values for hydrogenation of CO_2 to formate by a Ru(PNP) complex (1.1 M DBU base in DMF solvent, 40 atm of 3:1 H_2:CO_2).[11, 12] Based on this correlation, the Ru(PNP) catalyst would be expected to exhibit a TOF of 9400 h^{-1} at 25 °C.

References

1. C. R. Yonker and J. C. Linehan, *Prog. Nucl. Magn. Reson. Spectrosc.*, 2005, **47**, 95-109.
2. C. R. Yonker and J. C. Linehan, *J. Organomet. Chem.*, 2002, **650**, 249-257.
3. M. S. Jeletic, M. L. Helm, E. B. Hulley, M. T. Mock, A. M. Appel and J. C. Linehan, *ACS Catal.*, 2014, **4**, 3755-3762.
4. O. V. Dolomanov, L. J. Bourhis, R. J. Gildea, J. A. K. Howard and H. Puschmann, *Journal of Applied Crystallography*, 2009, **42**, 339-341.
5. G. M. Sheldrick, *Acta Crystallographica Section A*, 2015, **71**, 3-8.
6. G. M. Sheldrick, *Acta Crystallographica Section C*, 2015, **71**, 3-8.
7. D. J. Heldebrant, P. G. Jessop, C. A. Thomas, C. A. Eckert and C. L. Liotta, *J. Org. Chem.*, 2005, **70**, 5335-5338.
8. D. Kost, E. H. Carlson and M. Raban, *Journal of the Chemical Society D: Chemical Communications*, 1971, 656-657.
9. H. S. Gutowsky and C. H. Holm, *The Journal of Chemical Physics*, 1956, **25**, 1228-1234.
10. P. H. M. Budzelaar, gNMR (v. 5.0), IvorySoft, 1995-2006.
11. G. A. Filonenko, E. J. M. Hensen and E. A. Pidko, *Catal. Sci. Technol.*, 2014, **4**, 3474-3485.
12. G. A. Filonenko, R. van Putten, E. N. Schulpen, E. J. M. Hensen and E. A. Pidko, *ChemCatChem*, 2014, **6**, 1526-1530.